Unusual adsorption-induced phase transitions in a pillared-layered copper ethylenediphosphonate with ultrasmall channels

Margherita Cavallo,[1] Matteo Signorile,[1] Roberto Köferstein,[2] Valentina Crocellà,[1,*] Marco Taddei[3,4,5*]

[1] Dipartimento di Chimica, Centro di riferimento NIS e INSTM, Università di Torino, Via G. Quarello 15, I-10135 and Via P. Giuria 7, I-10125 Torino, Italy. Email: valentina.crocella@unito.it

[2] Institute of Chemistry, Inorganic Chemistry, Martin Luther University Halle-Wittenberg, Kurt-Mothes-Strasse 2, 06120 Halle, Germany

[3] Centro per l'Integrazione della Strumentazione Scientifica dell'Università di Pisa (CISUP), 56126 Pisa, Italy

[4] Dipartimento di Chimica e Chimica Industriale, Unità di Ricerca INSTM, Università di Pisa, Via Giuseppe Moruzzi 13, 56124 Pisa, Italy. Email: marco.taddei@unipi.it

[5] Energy Safety Research Institute, Swansea University, Fabian Way, Swansea, SA1 8EN UK

Electronic Supplementary Information

Contents

1. Crystal structure of Cu-EtP

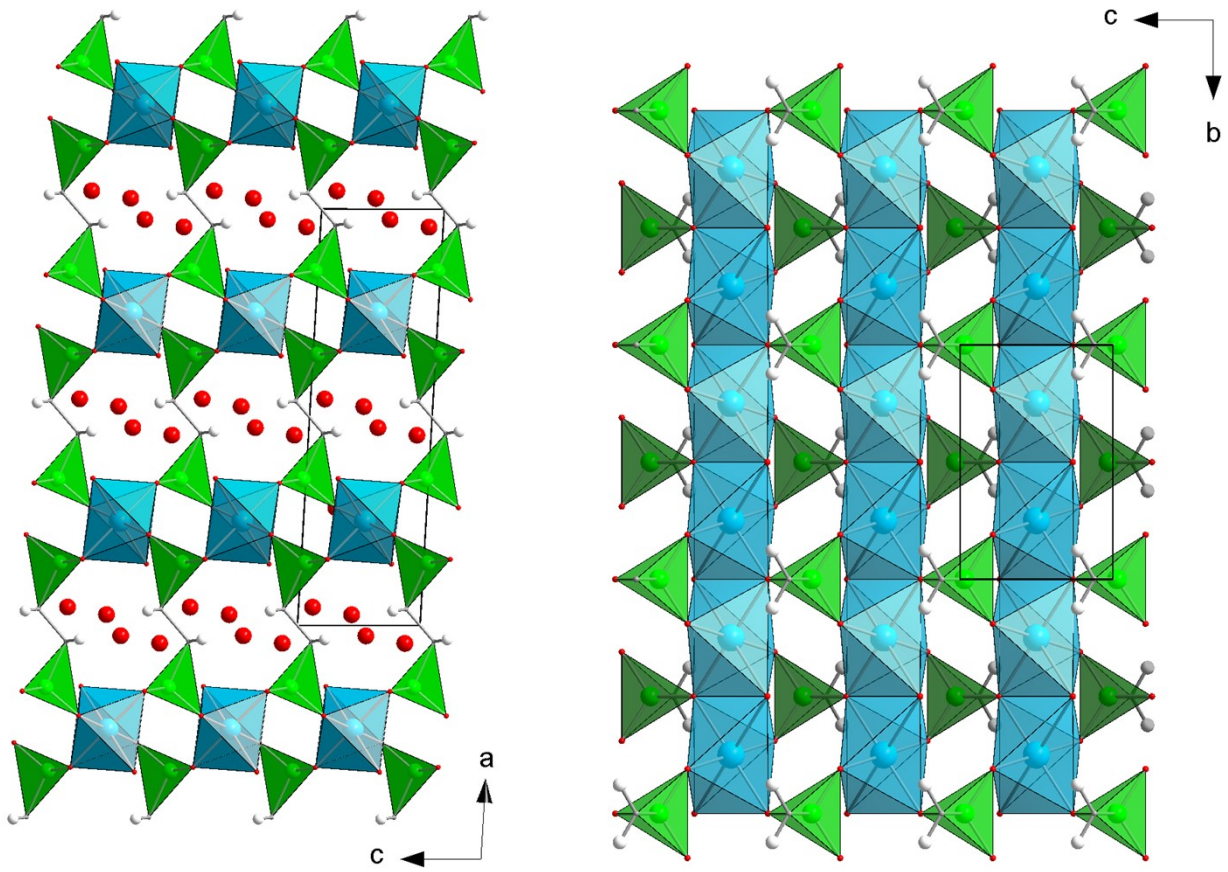

Figure S1. Polyhedral representation of the crystal structure of as synthesised Cu-EtP, viewed along the *b* axis (left), and of the structure of a single layer, viewed along the *a* axis (right). Colour code: Cu, cyan; P, green; C, grey; O, red; H, white.

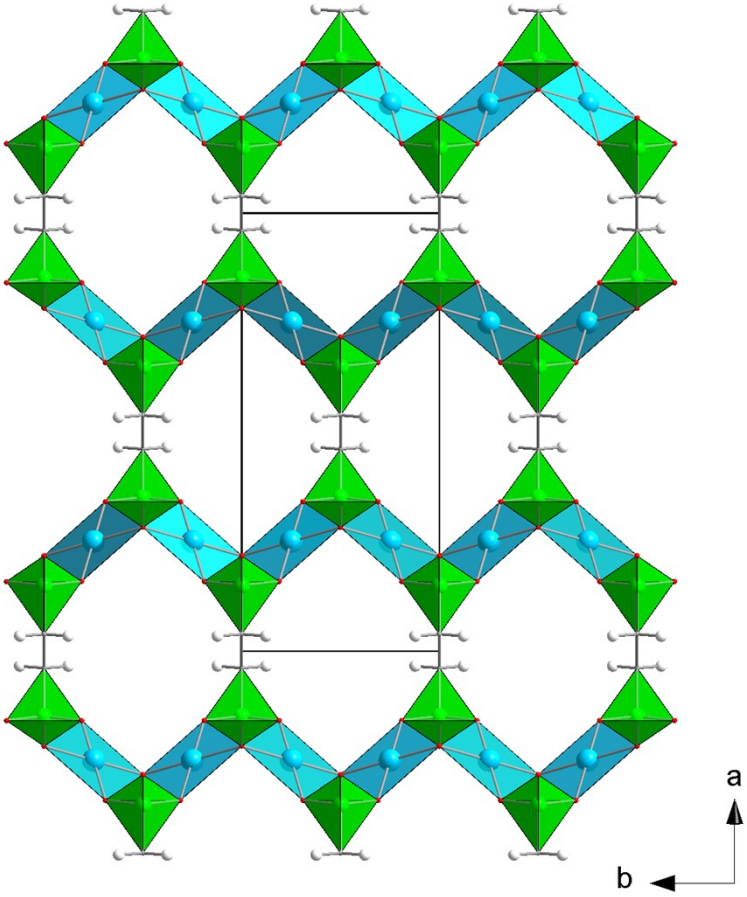

Figure S2. Polyhedral representation of the idealised crystal structure of evacuated Cu-EtP, viewed along the *c* axis. Colour code: Cu, cyan; P, green; C, grey; O, red; H, white.

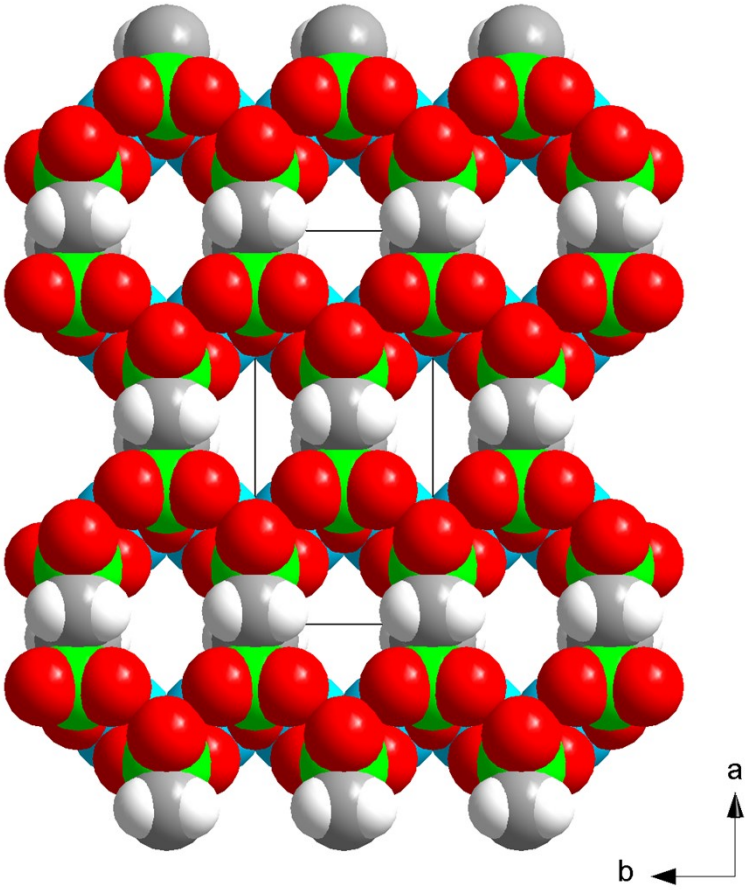

Figure S3. Space filling representation of the idealised crystal structure of evacuated Cu-EtP, viewed along the *c* axis. Colour code: Cu, cyan; P, green; C, grey; O, red; H, white.

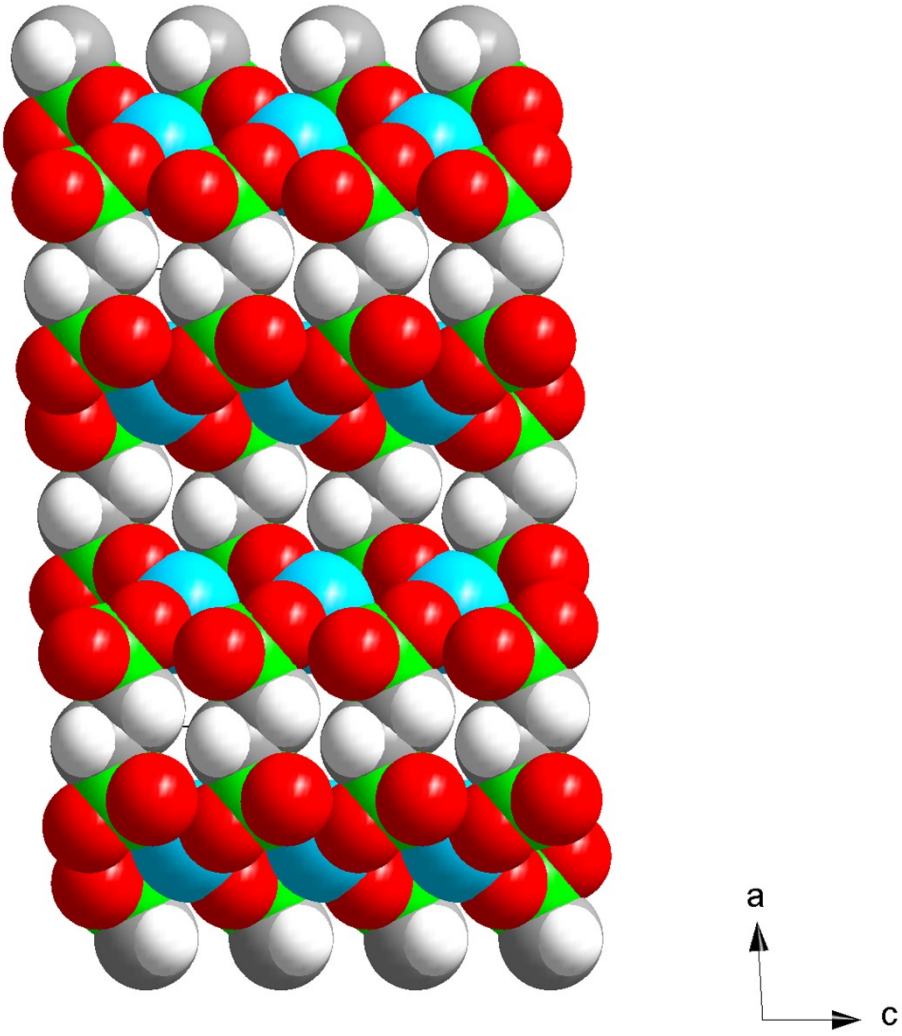

Figure S4. Space filling representation of the idealised crystal structure of evacuated Cu-EtP, viewed along the *b* axis. Colour code: Cu, cyan; P, green; C, grey; O, red; H, white.

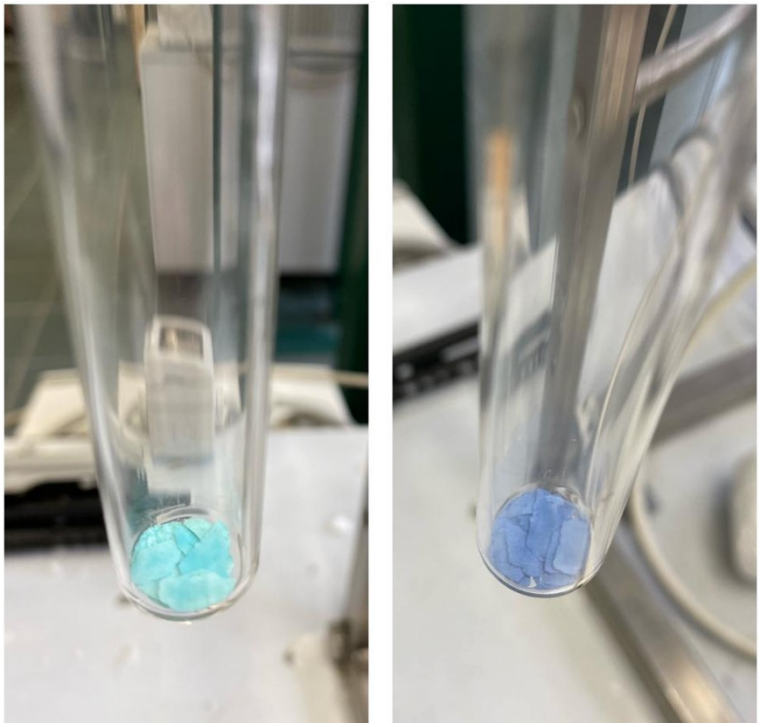

Figure S5. Colour change displayed by Cu-EtP as synthesised (left) and evacuated (right).

Table S1. Density of OMSs for Cu-EtP and some MOFs found in the literature. Formula weights and crystal densities are given for the desolvated compounds.

MOF	Formula	CSD refcode	Formula weight (g mol^{-1})	Crystal density (g mL^{-1})	OMSs density		
					mol kg^{-1}	mol L^{-1}	OMS Å^{-3}
Cu-EtP	Cu_2(EtP)	UXUPEK	313.1	2.41	12.8	30.8	0.0188
MOF-74(Mg)	Mg_2(dobdc)[a]	COKPEZ	244.6	0.92	8.2	7.6	0.0045
HKUST-1	$Cu_3(btc)_2$[b]	FIQCEN	604.7	0.88	4.9	4.3	0.0026
F4_MIL-140A(Ce)	CeO(tfbdc)[c]	LIGSAZ	392.1	2.20	2.5	5.5	0.0034
MAF-35	$Cu_2(OH)_2$(bdim)[d]	WIRMUH	319.1	1.37	12.6	17.2	0.0104

[a] dobdc^{2-} = 2,5-dihydroxyterephthalate; [b] btc^{3-} = trimesate; [c] tfbdc^{2-} = tetrafluoroterephthalate; [d] bdim^{2-} = benzodiimidazole

2. Gas sorption properties

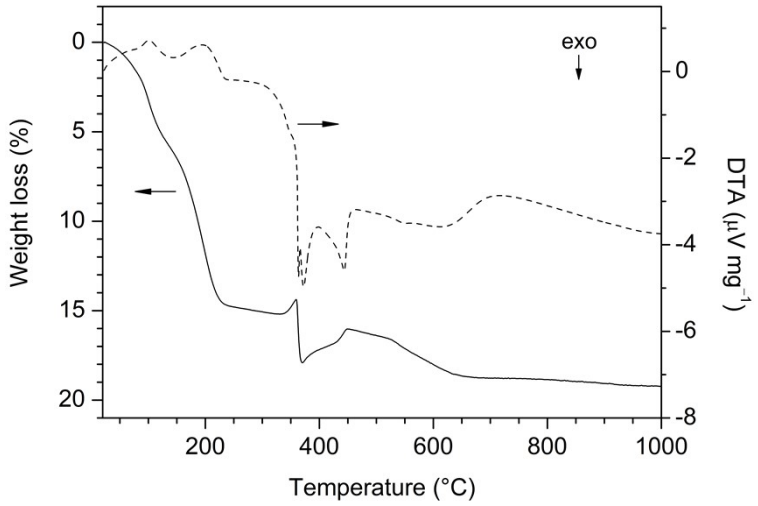

Figure S6. Thermogravimetric curve of Cu-EtP in air.

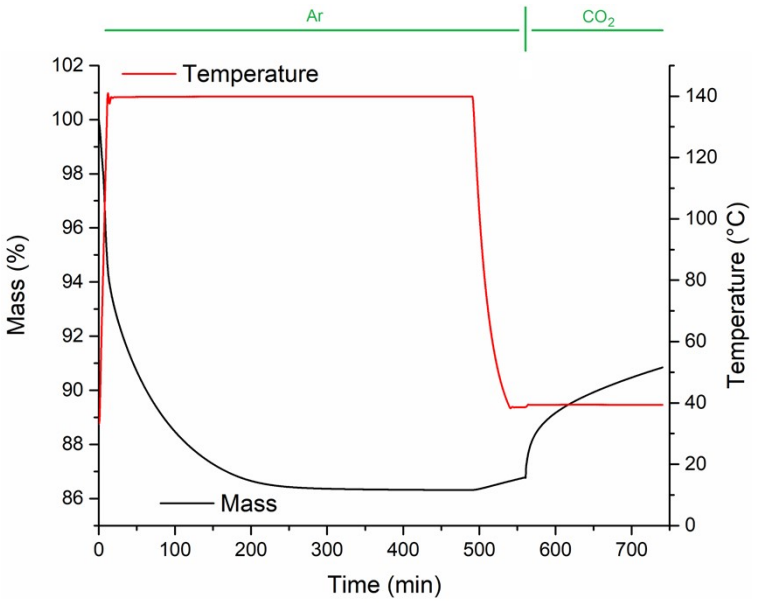

Figure S7. Thermogravimetric curve (black line) of Cu-EtP collected at different temperature (red line) and under a different atmosphere (green line): first, the solid was kept at 140 °C under Ar for 500 min; the temperature was then reduced to 40 °C and, once thermal equilibrium was reached, the sample was held under a 90:10 CO_2/Ar mixture.

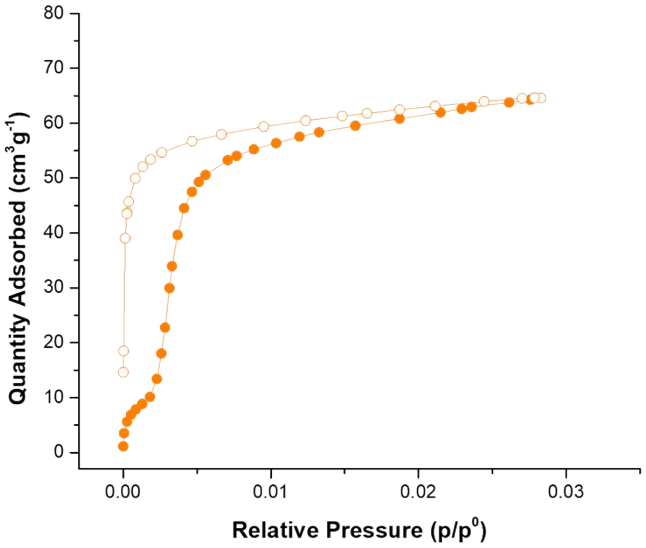

Figure S8. Volumetric adsorption/desorption isotherms, in $0 < p/p^0 < 0.03$ pressure range, of CO_2 at 273 K on Cu-EtP measured using an equilibration time of 60 s.

Table S2. Experimental data of the desorption branch of CO_2 isotherm measured using an equilibration time of 60 s used for the application of the BET equation.

p/p_0	p abs (mbar)	V ads (cm^3/g)	$p/V_m(p_0-p)$
2,83E-02	995,577	64,57950	0,00045075
2,79E-02	980,167	64,60970	0,000443366
2,70E-02	951,229	64,51720	0,000430529
2,45E-02	860,581	63,96670	3,9E-04
0,02112	743,286	63,11040	0,000341837
0,01872	658,961	62,45730	0,000305477
0,01651	581,075	61,80400	0,000271606
0,01484	522,286	61,28760	0,000245767
0,01236	434,993	60,46130	0,000206966
0,00952	335,226	59,35770	0,000161999
0,00666	234,352	57,97110	0,000115625
0,00466	164,164	56,68940	8,2661E-05

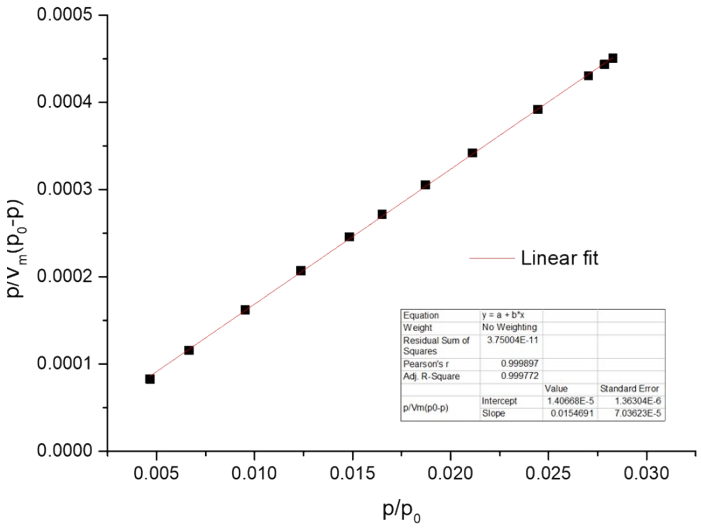

Figure S9. Linear BET fit in the $0.005<p/p_0<0.030$ pressure range for CO_2 desorption isotherm at 273 K measured using an equilibration time of 60 s.

Table S3. Slope (B) and intercept (A) parameters obtained from the linear BET fit and the computed V_m (monolayer capacity), c (BET constant) and S_a (Specific Surface Area) values.

A= 0,0000140	B=0,01547
$A = 1/c \cdot V_m$	$B= (c-1)/c \cdot Vm$
V_m (cm^3/g)$=1/(((B/A)+1) \cdot A)$	$c=(B/A)+1$
V_m=64,58279514	c=1.106
S_a (m^2 /g)= $(\boldsymbol{Vm} \cdot \boldsymbol{N} \cdot \boldsymbol{\sigma s})/(\boldsymbol{22414} \cdot \boldsymbol{m})$=294,9763126	

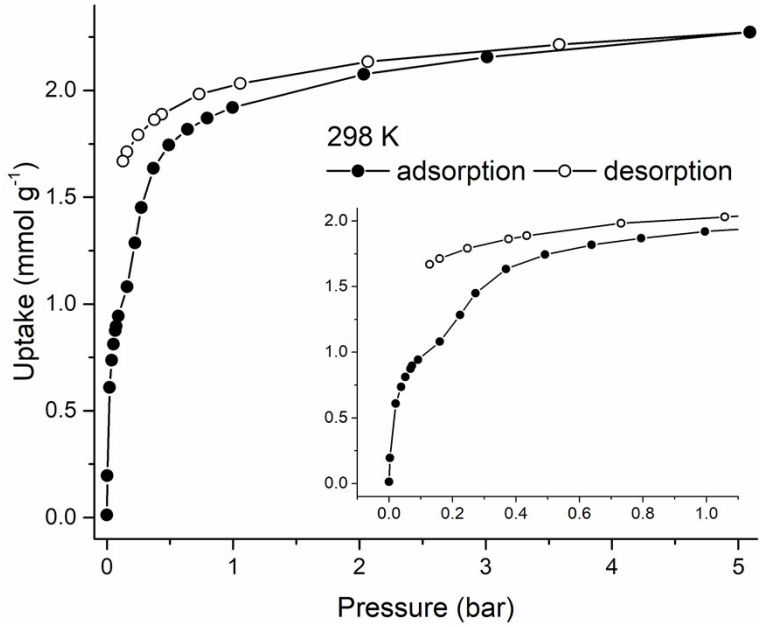

Figure S10. CO_2 adsorption/desorption isotherms collected on Cu-EtP at 298 K up to 5 bar.

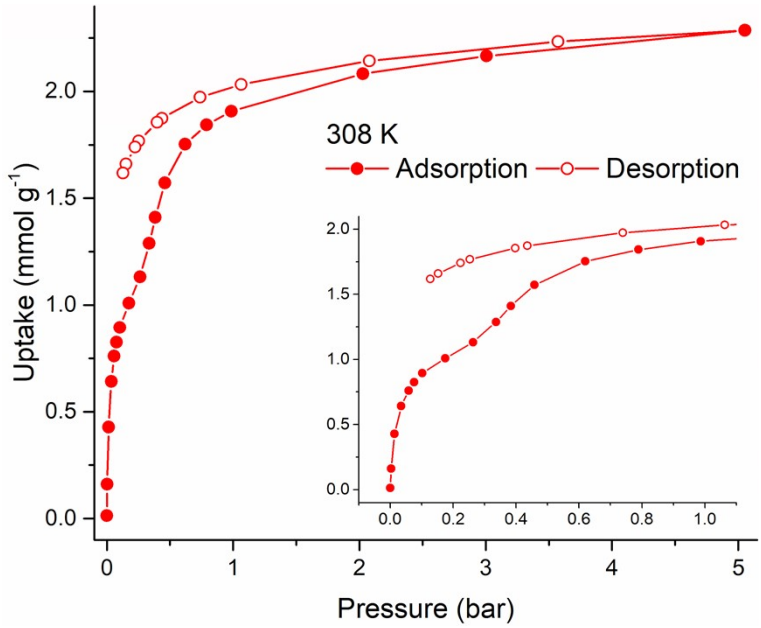

Figure S11. CO_2 adsorption/desorption isotherms collected on Cu-EtP at 308 K up to 5 bar.

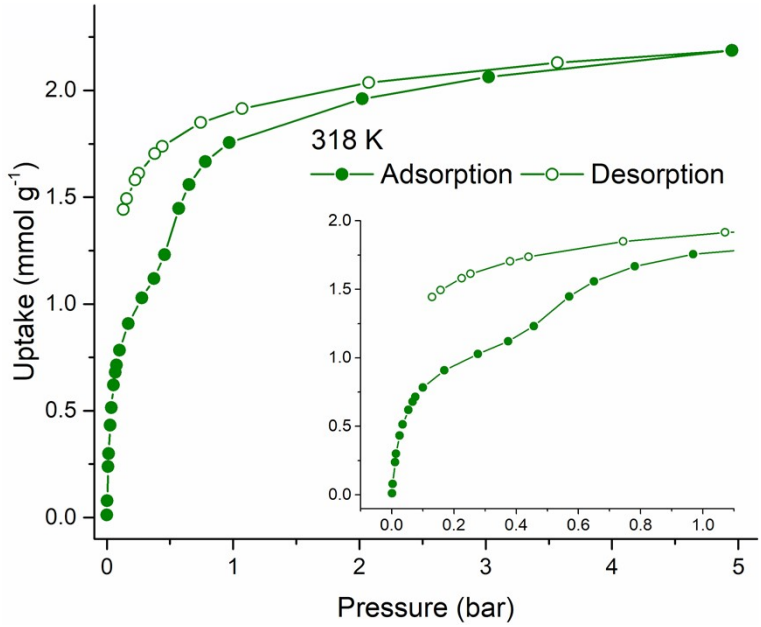

Figure S12. CO_2 adsorption/desorption isotherms collected on Cu-EtP at 318 K up to 5 bar.

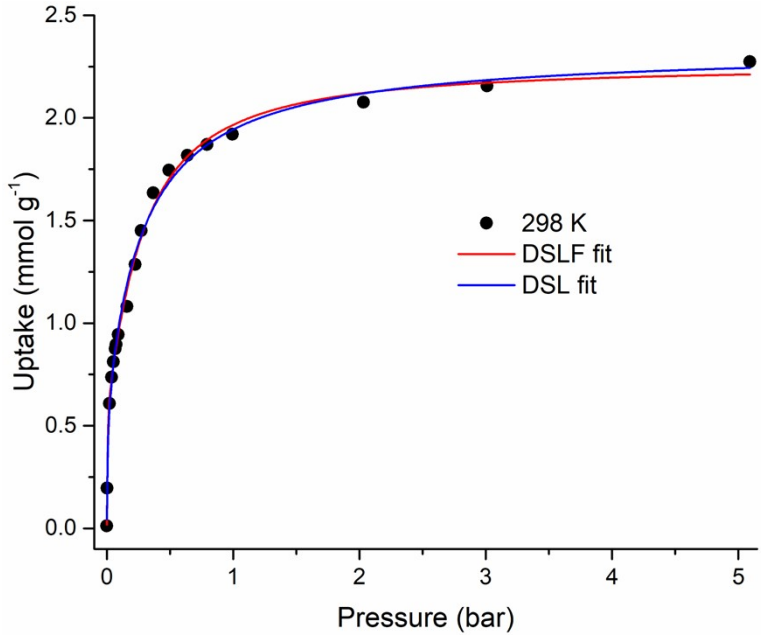

Figure S13. Dual site Langmuir Freundlich (DSLF) fit (red line) and Dual site Langmuir (DSL) fit (blue line) of the CO_2 adsorption isotherm collected at 298 K (black circles) up to 5 bar.

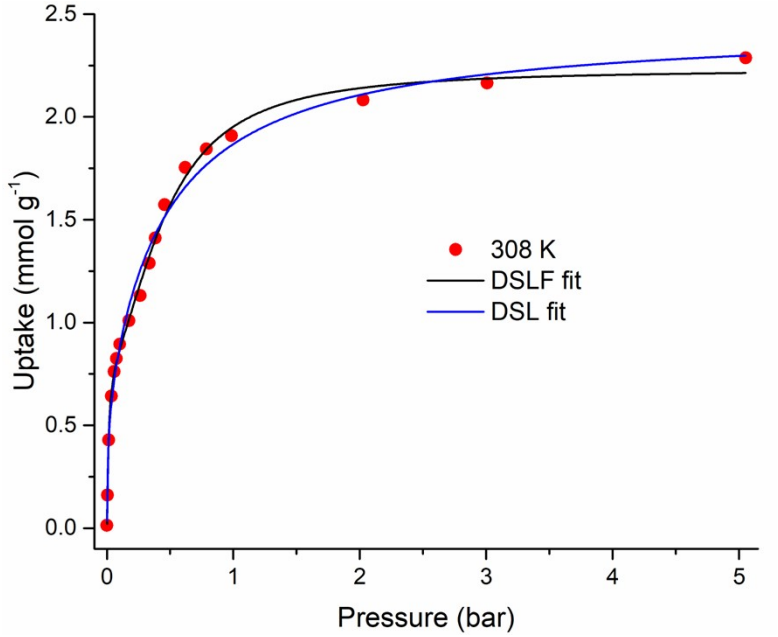

Figure S14. Dual site Langmuir Freundlich (DSLF) fit (black line) and Dual site Langmuir (DSL) fit (blue line) of the CO_2 adsorption isotherm collected at 308 K (red circles) up to 5 bar.

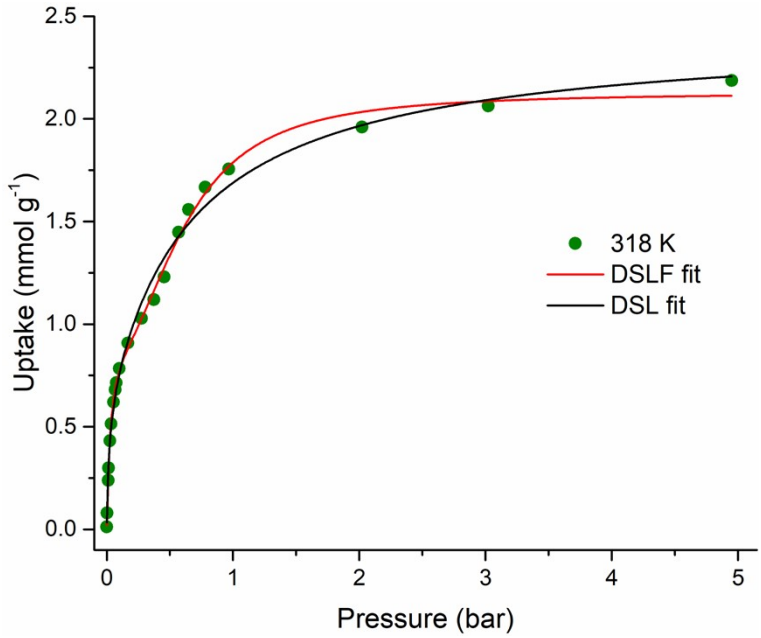

Figure S15. Dual site Langmuir Freundlich (DSLF) fit (black line) and Dual site Langmuir (DSL) fit (blue line) of the CO_2 adsorption isotherm collected at 318 K (green circles) up to 5 bar.

Table S4. Dual site Langmuir Freundlich fitting parameters of the CO_2 adsorption isotherms collected at 298 K, 308 K and 318 K up to 5 bar. Uptake values expressed in mol g^{-1}.

Temperature (K)	q_1	k_1	n_1	q_2	k_2	n_2	R^2
298	0.0016 ± 2E-4	3.5 ± 0.6	1.2 ± 0.2	6E-4 ± 2E-4	180 ± 104	1.4 ± 0.8	0.99553
308	0.0014 ± 1 E-4	2.1 ± 0.2	1.8 ± 0.3	9E-4 ± 1E-4	70 ± 25	1.1 ± 0.3	0.99619
318	0.0012 ± 1E-4	1.6 ± 0.1	2.2 ± 0.4	9E-4 ± 1 E-4	34 ± 10	1.1 ± 0.2	0.99694

Table S5. Dual site Langmuir fitting parameters of the CO_2 adsorption isotherms collected at 298 K, 308 K and 318 K up to 5 bar. Uptake values expressed in mol g^{-1}.

Temperature (K)	q_1	k_1	q_2	k_2	R^2
298	0.00176 ± 7E-5	3.5 ± 0.5	5.8E-4 ± 8E-5	170 ± 78	0.99497
308	0.00188 ± 9E-5	2.2 ± 0.4	6E-4 ± 1E-4	128 ± 71	0.99189
318	0.00182 ± 9E-5	1.5 ± 0.3	6E-4 ± 1E-4	58 ± 25	0.9927

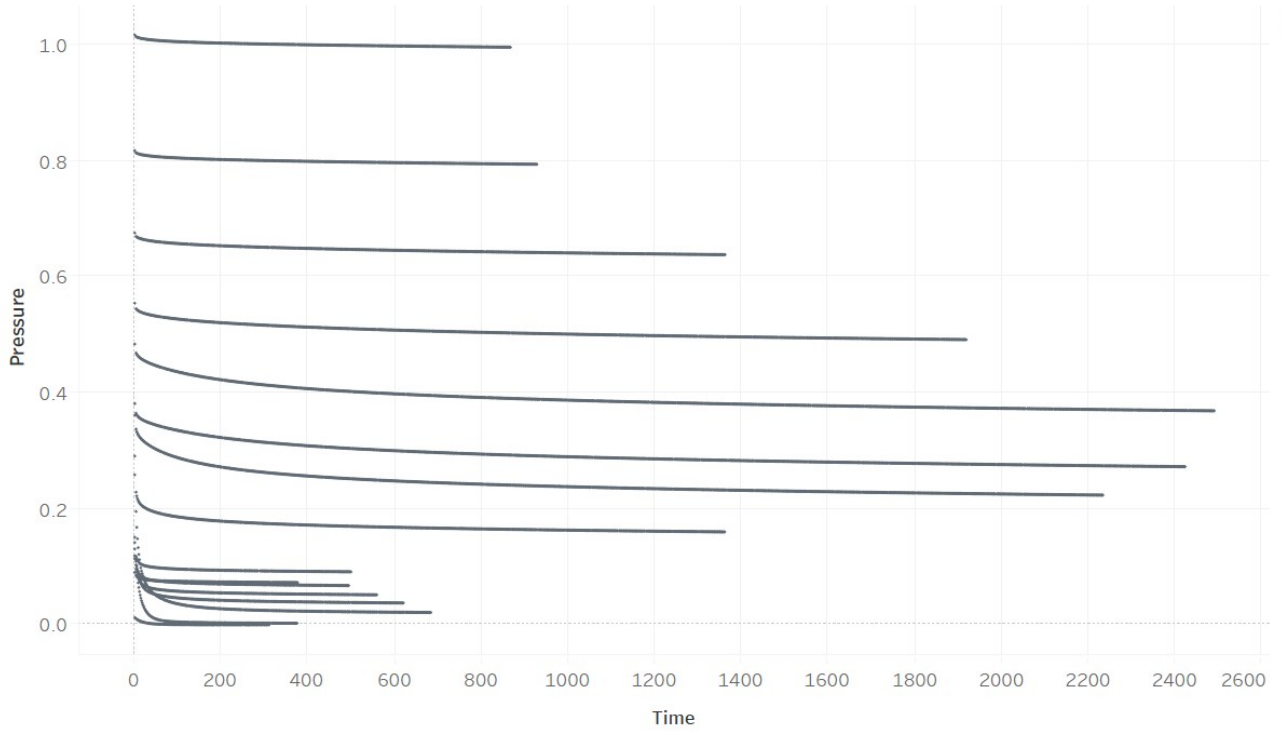

Figure S16. Variation of pressure in the sample cell as a function of time after each gas dose during the isotherm collected at 298 K.

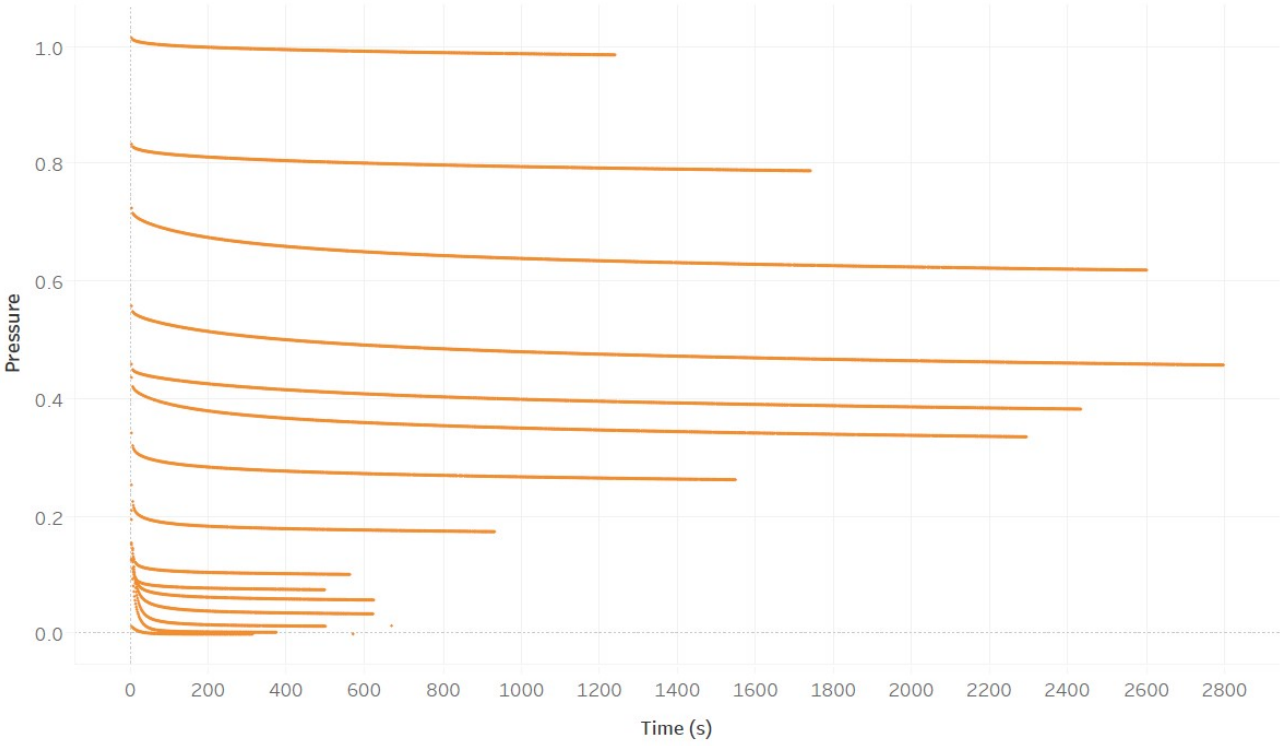

Figure S17. Variation of pressure in the sample cell as a function of time after each gas dose during the isotherm collected at 308 K.

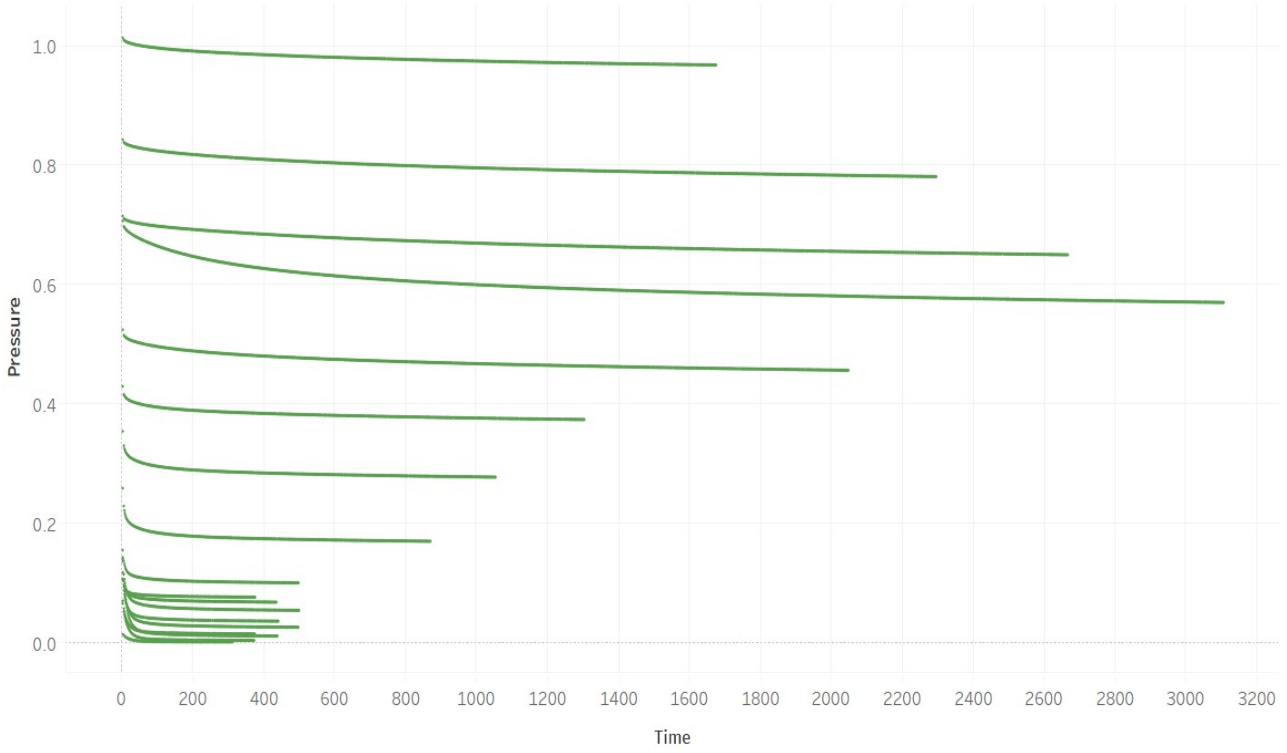

Figure S18. Variation of pressure in the sample cell as a function of time after each gas dose during the isotherm collected at 318 K.

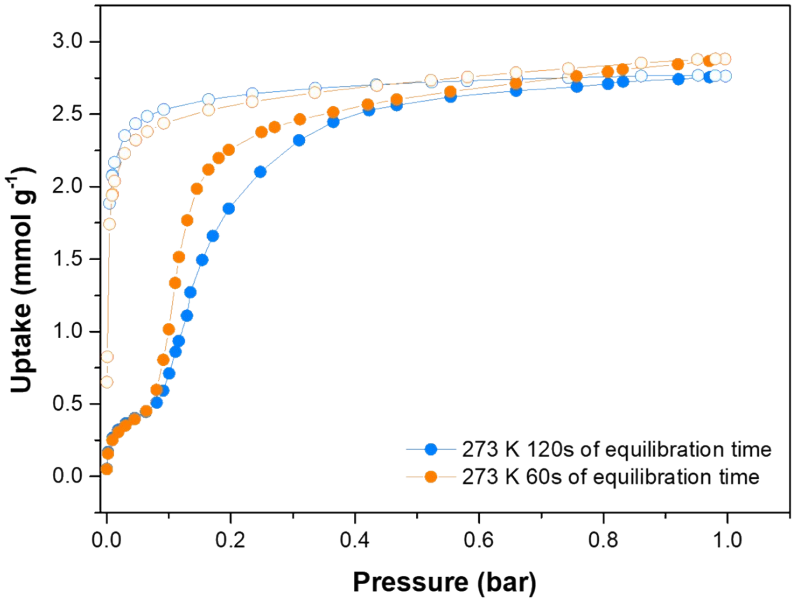

Figure S19. Volumetric adsorption/desorption isotherms of CO_2 at 273 K on Cu-EtP with 60 seconds (orange) and 120 seconds (light blue) of equilibration time.

Table S6. Experimental data of the desorption branch of CO_2 isotherm measured using an equilibration time of 120 s used for the application of the BET equation.

p/p_0	p abs (mbar)	V ads (cm^3/g)	$p/V_m(p_0-p)$
0,02831	996	61,9492	0,000470319
0,02784	980	61,985	0,000462
0,02706	952,454	62,056	0,000448197
0,02445	860,548	61,9295	0,00040469
0,02112	743,38	61,6949	0,000349725
0,01876	660,352	61,4889	0,000310956
0,01649	580,515	61,1962	0,000274035
0,01487	523,363	61,0049	0,000247422
0,01233	433,907	60,6103	0,000205936
0,00954	335,835	60,0619	0,000160393
0,00666	234,541	59,1979	0,000113321
0,00466	164,088	58,3188	8,03141E-05

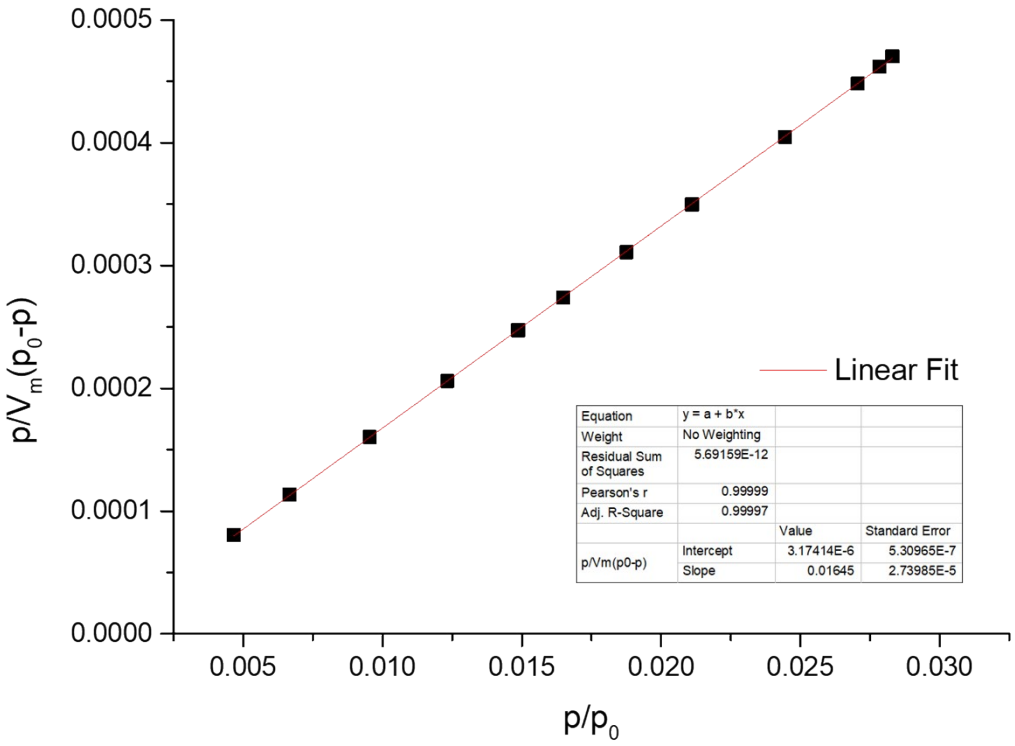

Figure S20. Linear BET fit in the $0.005<p/p_0<0.030$ pressure range for CO_2 desorption isotherm at 273 K measured using an equilibration time of 120 s.

Table S7. Slope (B) and intercept (A) parameters obtained from the linear BET fit and the computed V_m (monolayer capacity), c (BET constant) and S_a (Specific Surface Area) values.

A=0,0000032	B=0,01645
$A = 1/c \cdot V_m$	$B= (c-1)/c \cdot Vm$
V_m (cm^3/g)=1/(((B/A)+1)·A)	c=(B/A)+1
V_m=60,77845039	c=5.142
S_a (m^2 /g)= $(\boldsymbol{Vm} \cdot \boldsymbol{N} \cdot \boldsymbol{\sigma s})/(\boldsymbol{22414} \cdot \boldsymbol{m})$=277,6002981	

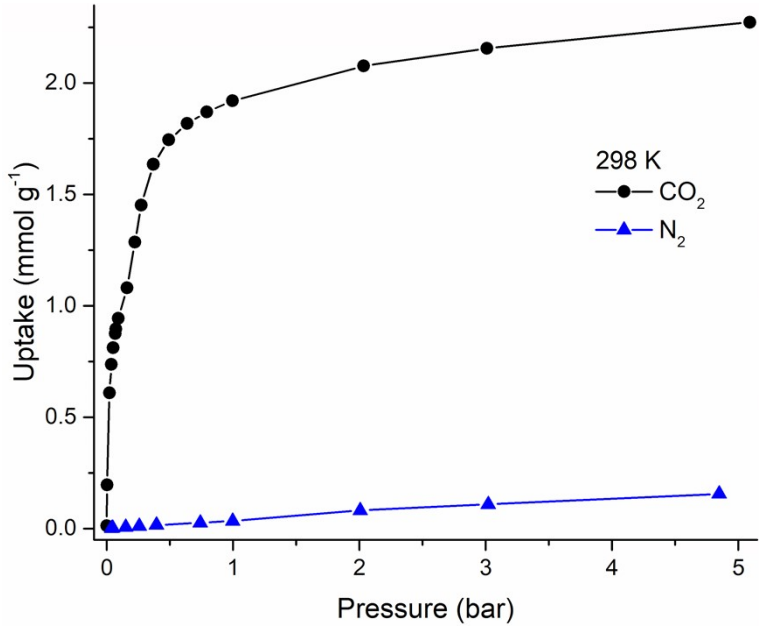

Figure S21. Comparison of CO_2 (black) and N_2 (blue) adsorption isotherms collected on Cu-EtP at 298 K up to 5 bar.

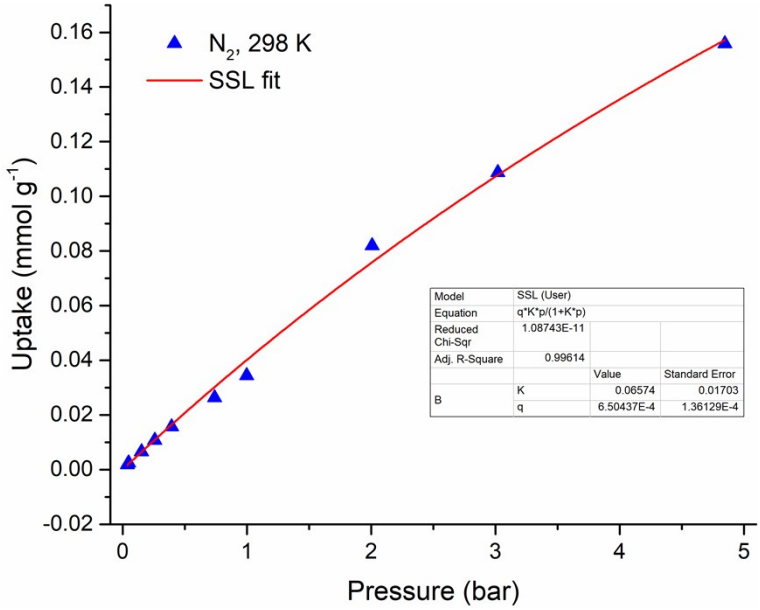

Figure S22. Single site Langmuir (SSL) fit (red line) of the N_2 adsorption isotherm collected at 298 K (blue triangles) up to 5 bar.

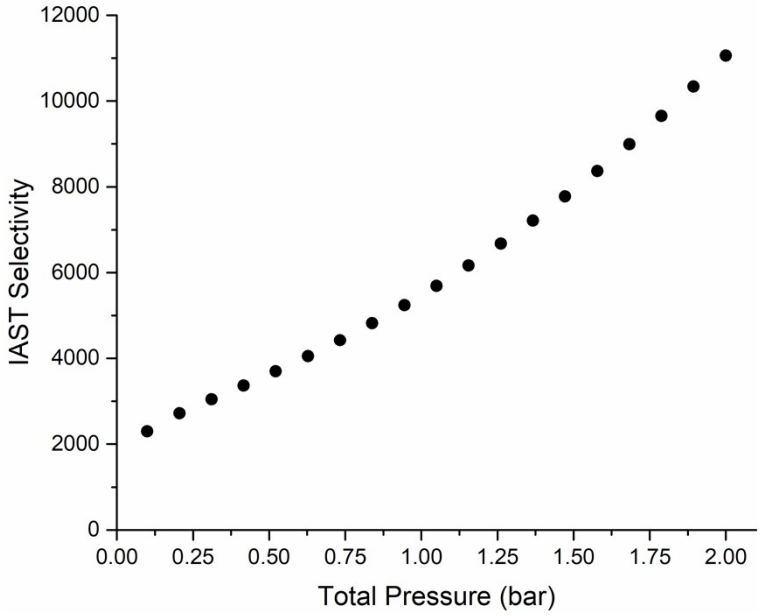

Figure S23. Calculated IAST selectivity as a function of total pressure for a 85:15 N_2/CO_2 mixture.

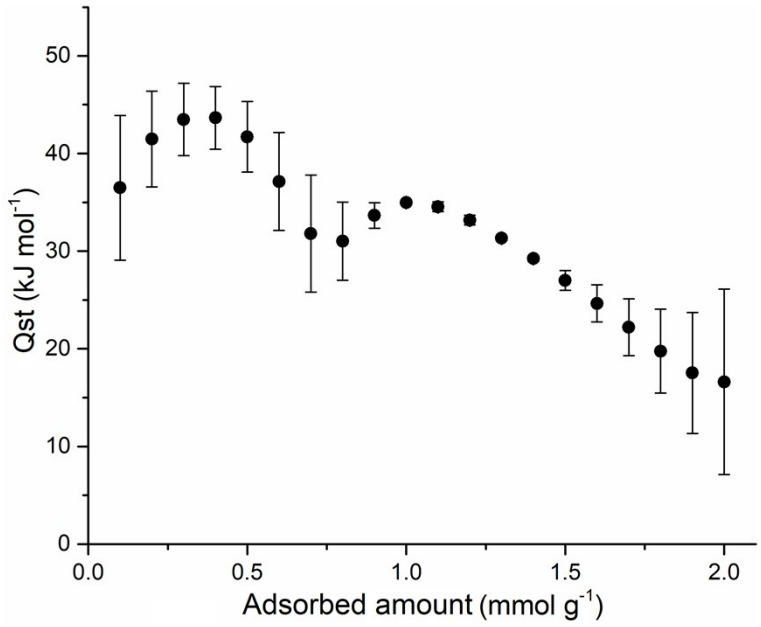

Figure S24. Plot of isosteric heat of CO_2 adsorption (Qst) versus loading obtained from the isotherms collected at 298 K, 303 K, 318 K and 343 K up to 5 bar.

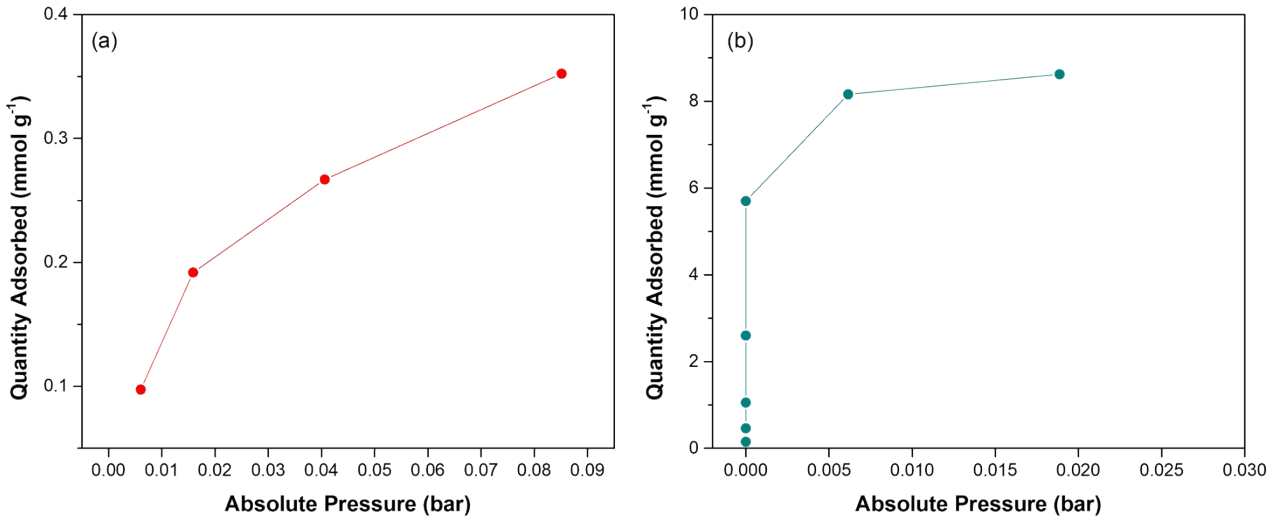

Figure S25. Adsorption isotherms of CO_2 at 308 K (a) and H_2O at 303 K (b) obtained with the volumetric line coupled with the microcalorimeter on Cu-EtP. The corresponding differential molar adsorption heats curves are reported in Figure 3 in the main text.

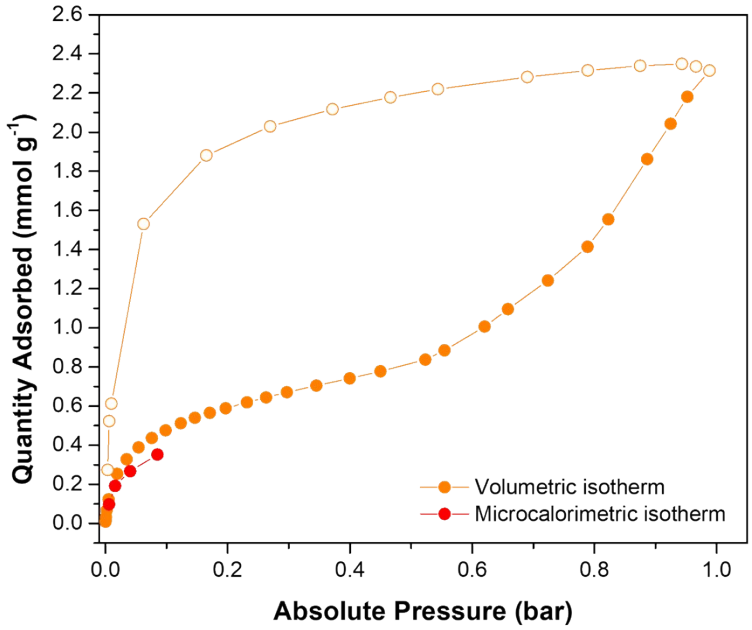

Figure S26. Comparison of volumetric isotherms obtained by performing CO_2 adsorption at 308 K on Cu-EtP (using 60s of equilibration) time with the automatic volumetric instrument (orange) and with the volumetric line coupled with the microcalorimeter (red).

3. *In situ* powder X-ray diffraction (PXRD)

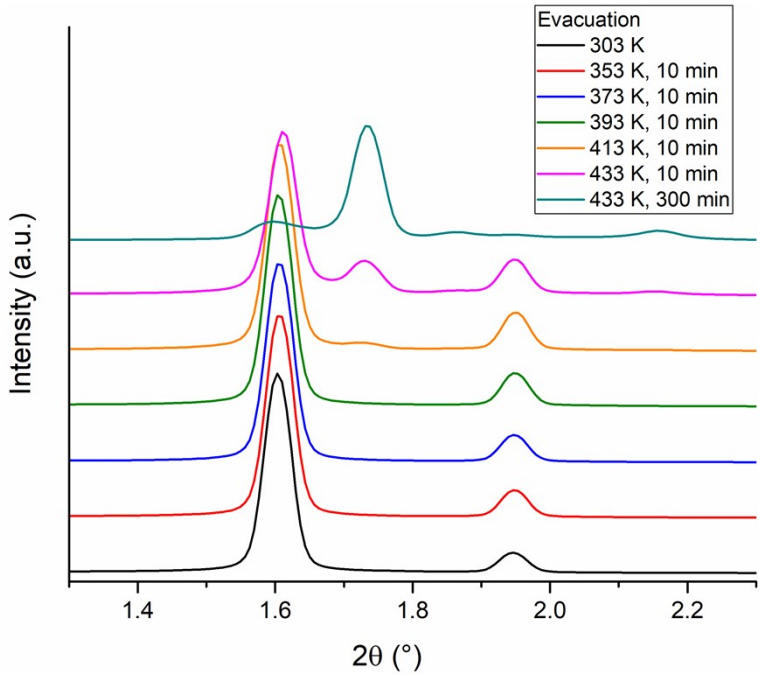

Figure S27. Low angle region of the PXRD pattern of as synthesised Cu-EtP during the evacuation process at progressively increasing temperature.

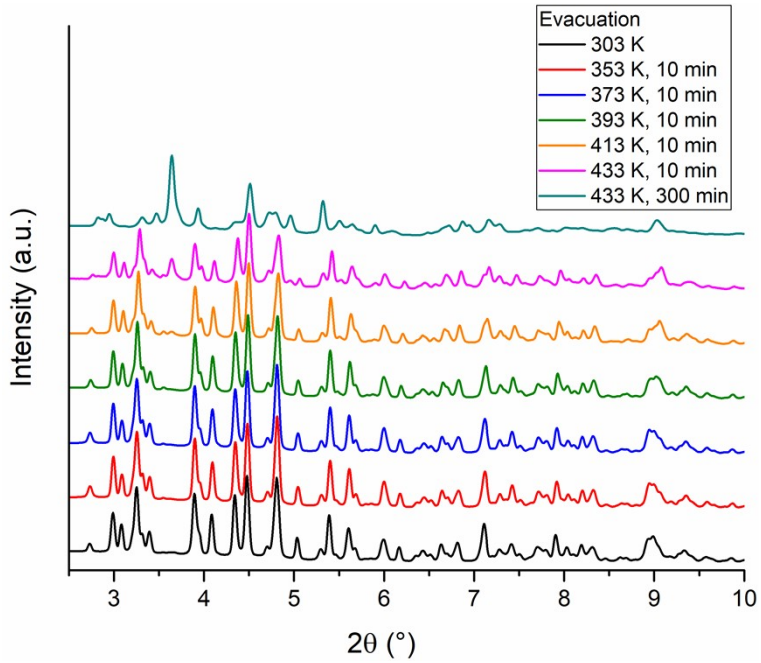

Figure S28. High angle region of the PXRD pattern of as synthesised Cu-EtP during the evacuation process at progressively increasing temperature.

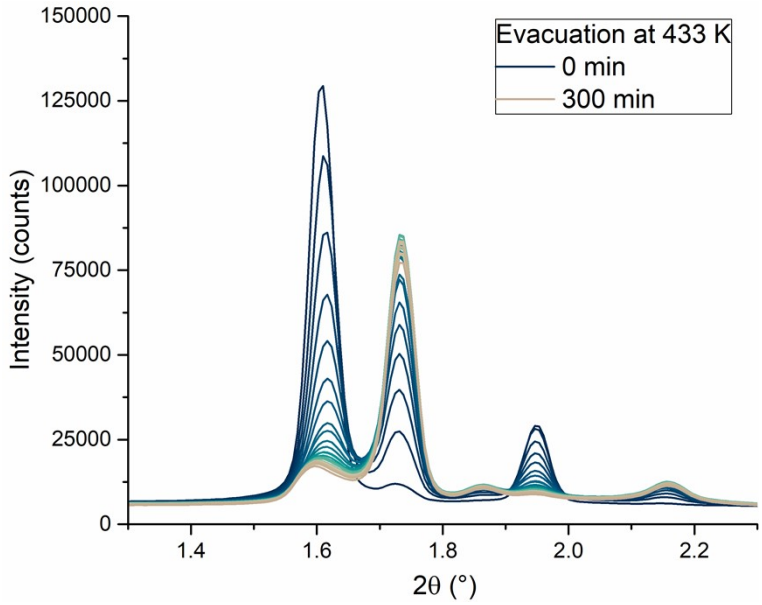

Figure S29. Low angle region of the PXRD pattern of as synthesised Cu-EtP held at 433 K for 300 minutes.

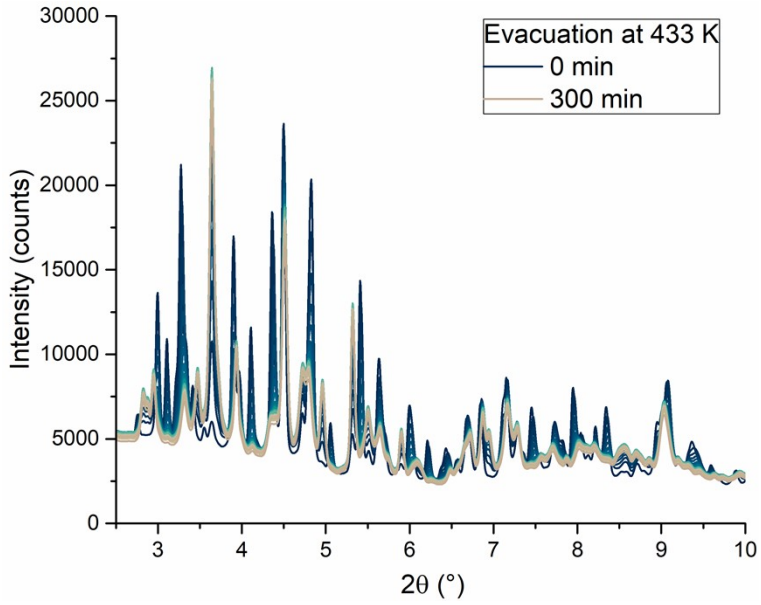

Figure S30. High angle region of the PXRD pattern of as synthesised Cu-EtP held at 433 K for 300 minutes.

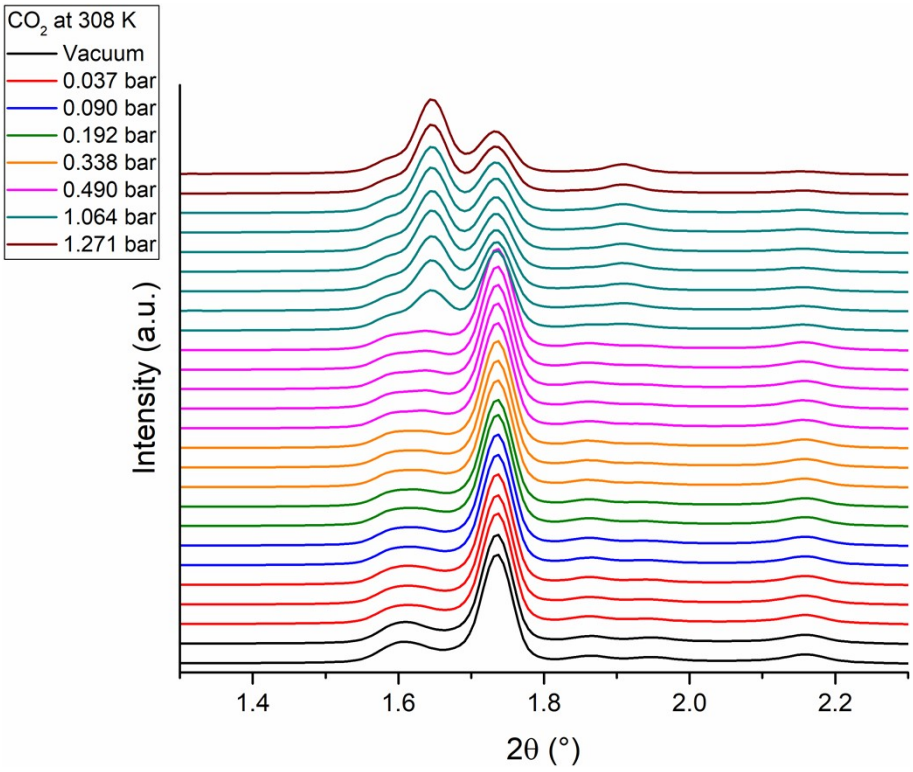

Figure S31. Low angle region of the PXRD pattern of evacuated Cu-EtP exposed to increasing pressures of CO_2 at 308 K. Patterns at the same temperature were collected every five minutes.

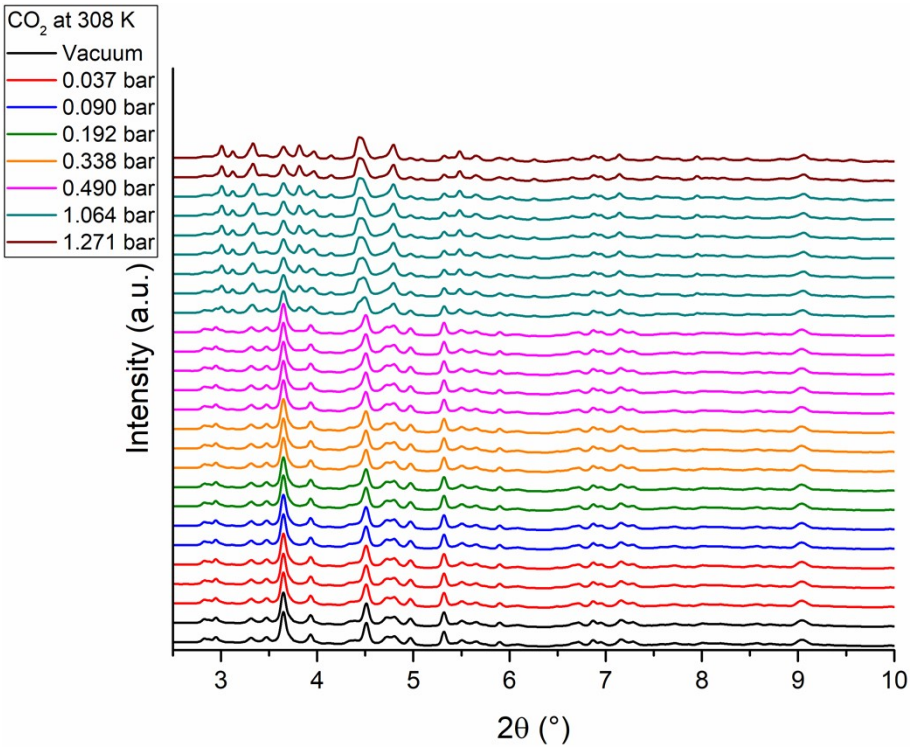

Figure S32. High angle region of the PXRD pattern of evacuated Cu-EtP exposed to increasing pressures of CO_2 at 308 K. Patterns at the same temperature were collected every five minutes.

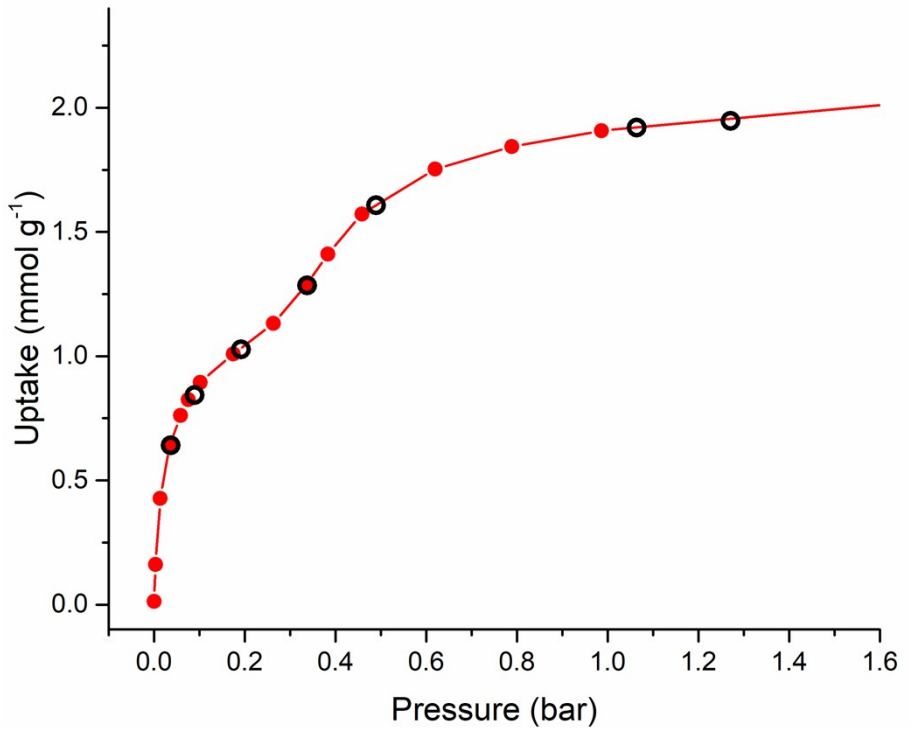

Figure S33. Visualisation of the pressures explored during the *in situ* experiment of Figures S30-31 (black circles), with respect to the adsorption isotherm collected at 308 K.

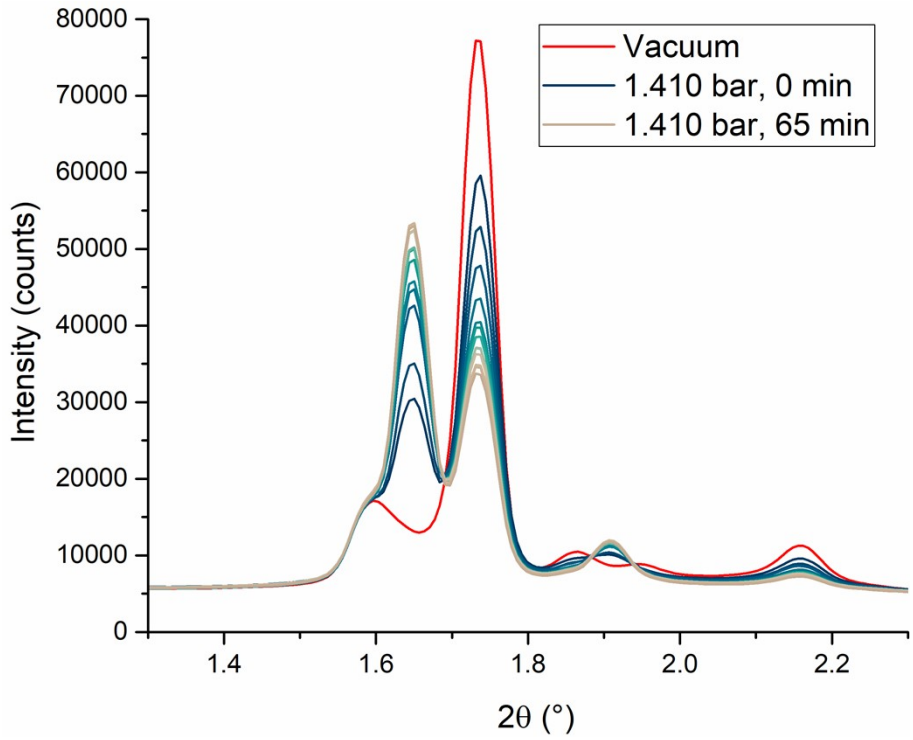

Figure S34. Low angle region of the PXRD pattern of evacuated Cu-EtP held under a constant pressure of 1.410 bar of CO_2 at 308 K.

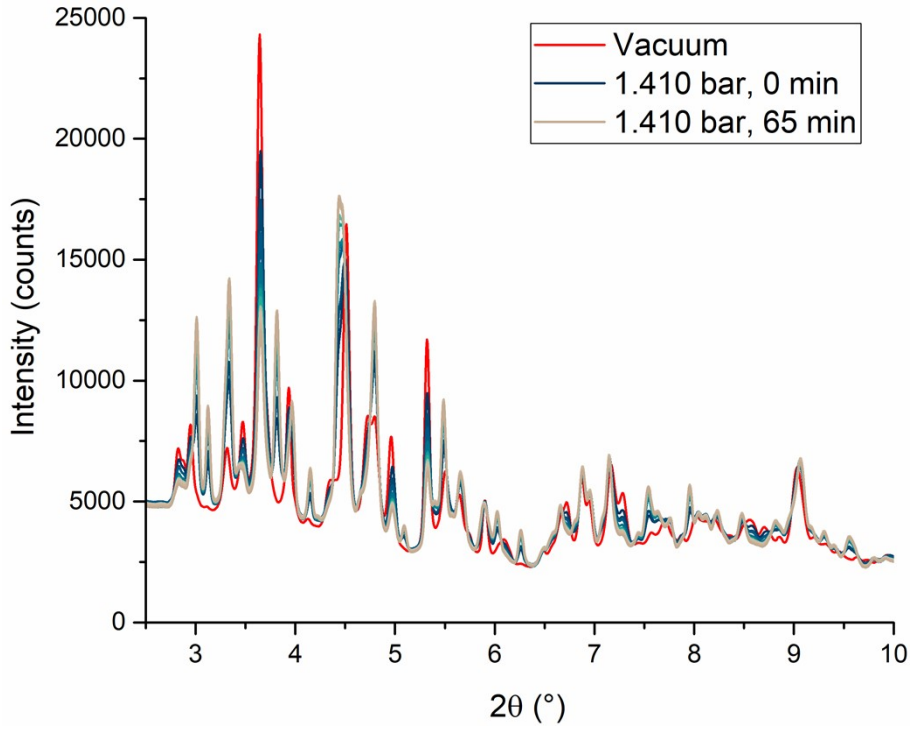

Figure S35. High angle region of the PXRD pattern of evacuated Cu-EtP held under a constant pressure of 1.410 bar of CO_2 at 308 K.

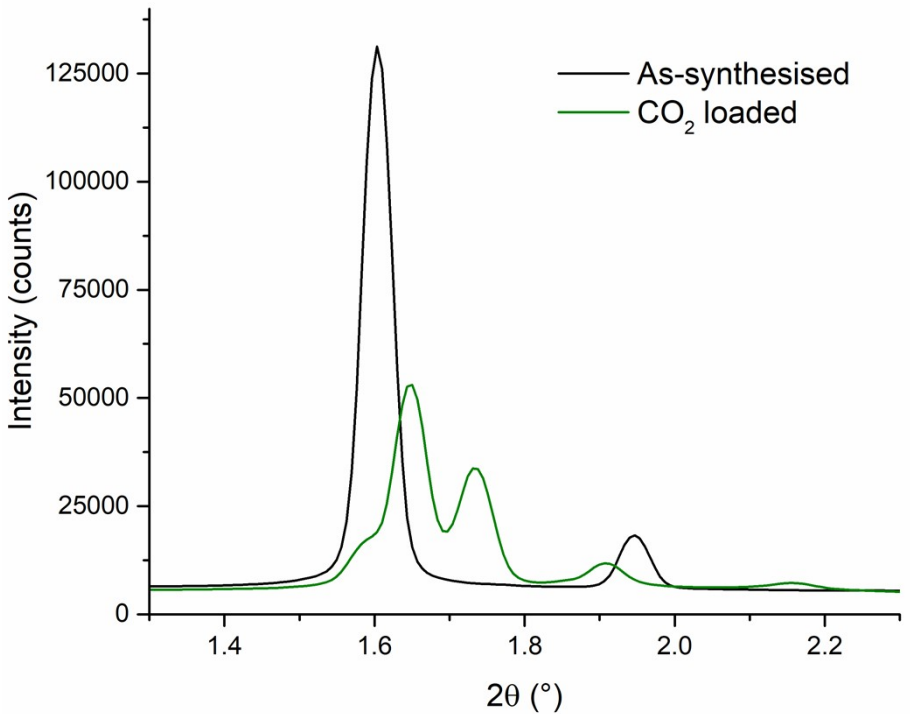

Figure S36. Comparison of the low angle region of the PXRD patterns of as synthesised (black) and CO_2 loaded (green) Cu-EtP.

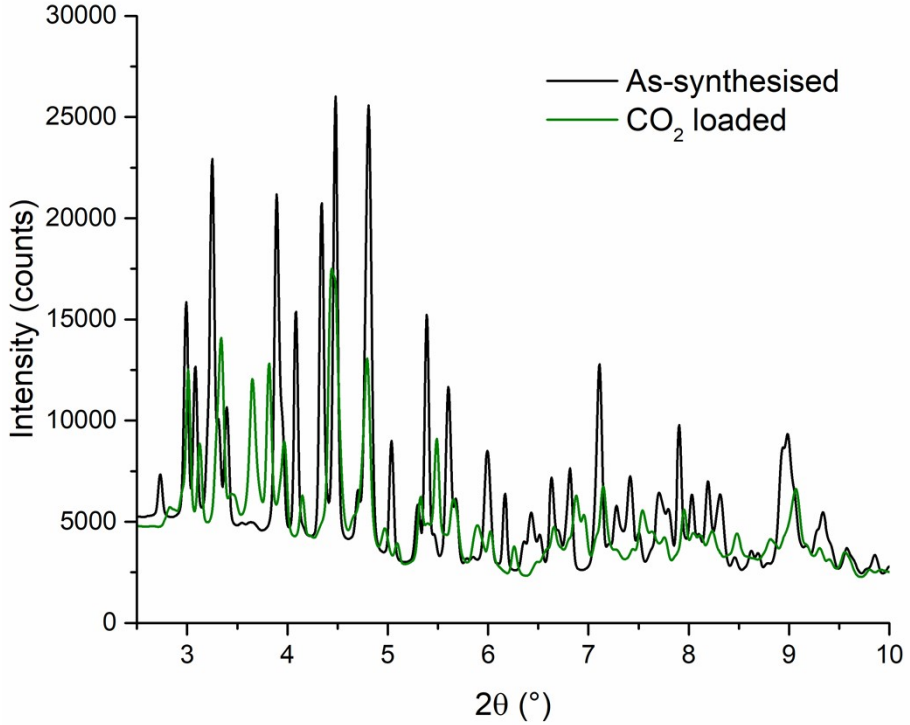

Figure S37. Comparison of the high angle region of the PXRD patterns of as synthesised (black) and CO_2 loaded (green) Cu-EtP.

4. *In situ* infrared (IR) spectroscopy

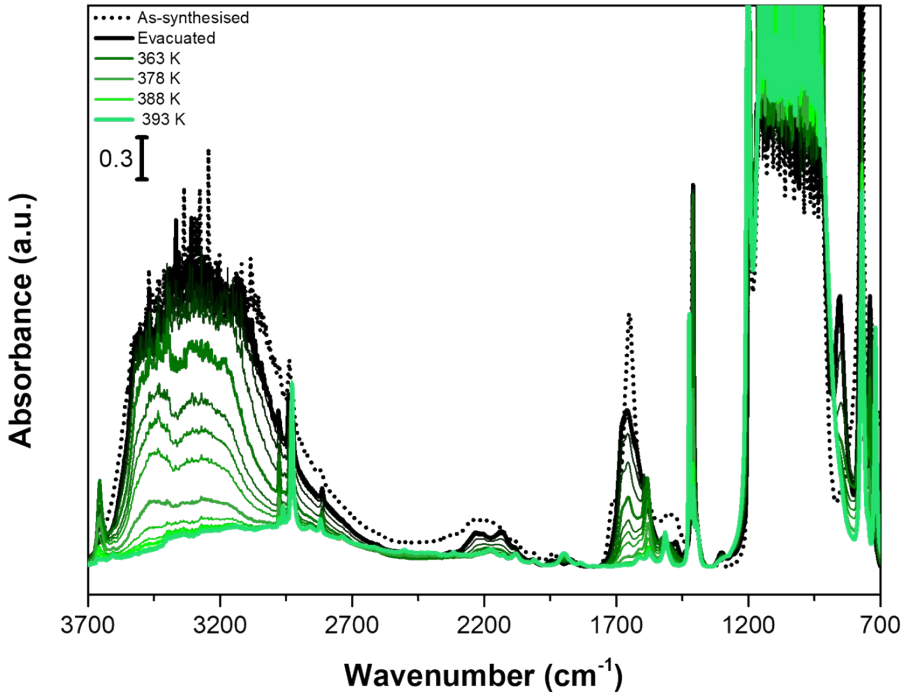

Figure S38. IR spectra of Cu-EtP collected in the 313-393 K temperature range, reported in the full spectral range after a baseline correction. Dashed black curve represents the as synthesised Cu-EtP, black curve represents the evacuated sample, green curves represent Cu-EtP spectra at increasing temperatures.

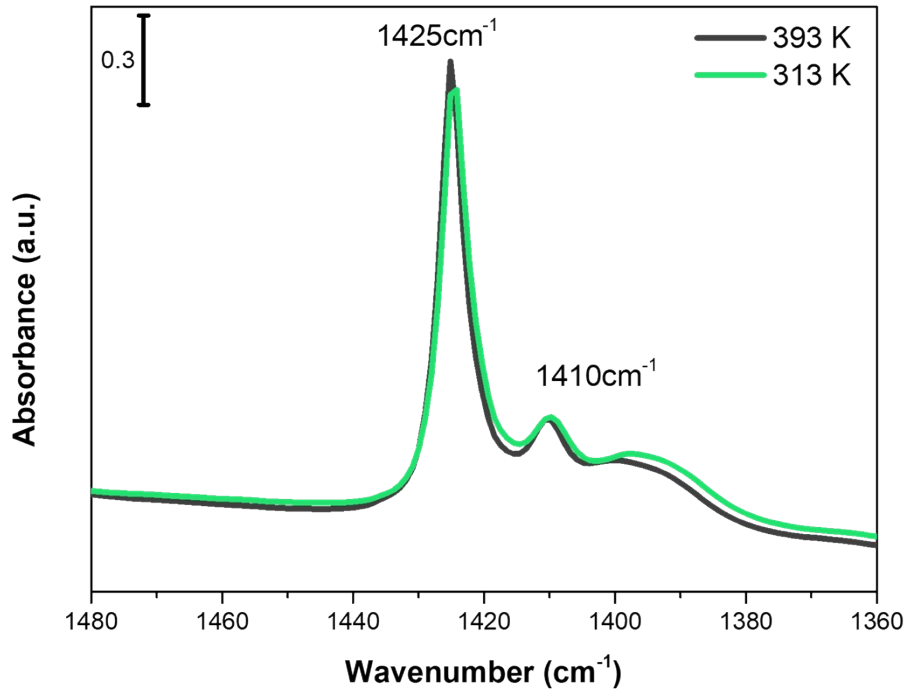

Figure S39. IR spectra of Cu-EtP collected at 393 K and after cooling down to 313 K.

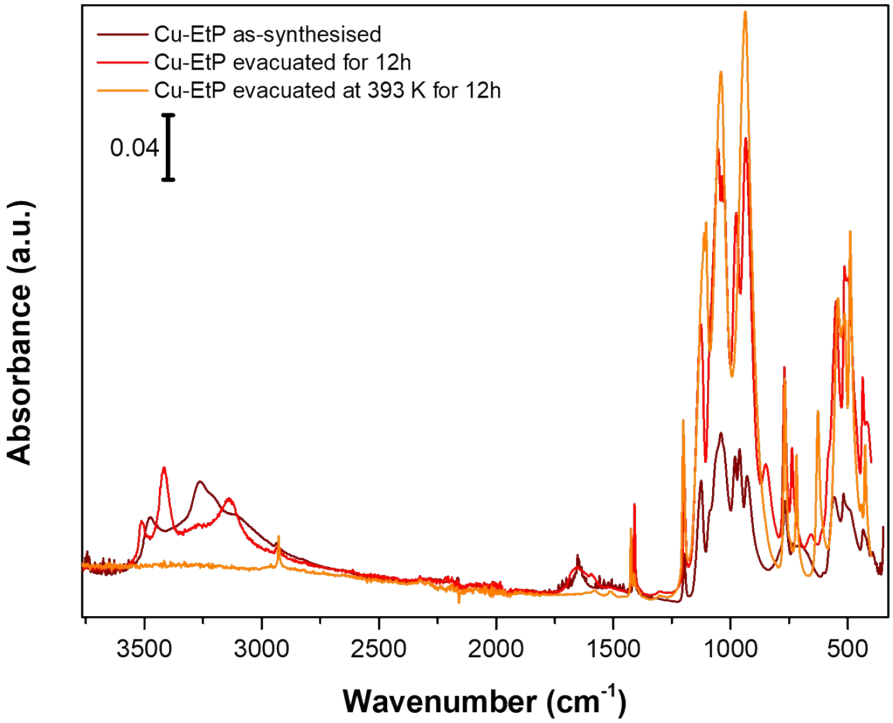

Figure S40. ATR-IR spectra of Cu-EtP collected on the as synthesised sample (wine), on the sample evacuated for 12 h (red) and on the sample evacuated at 393 K for 12 h (orange).

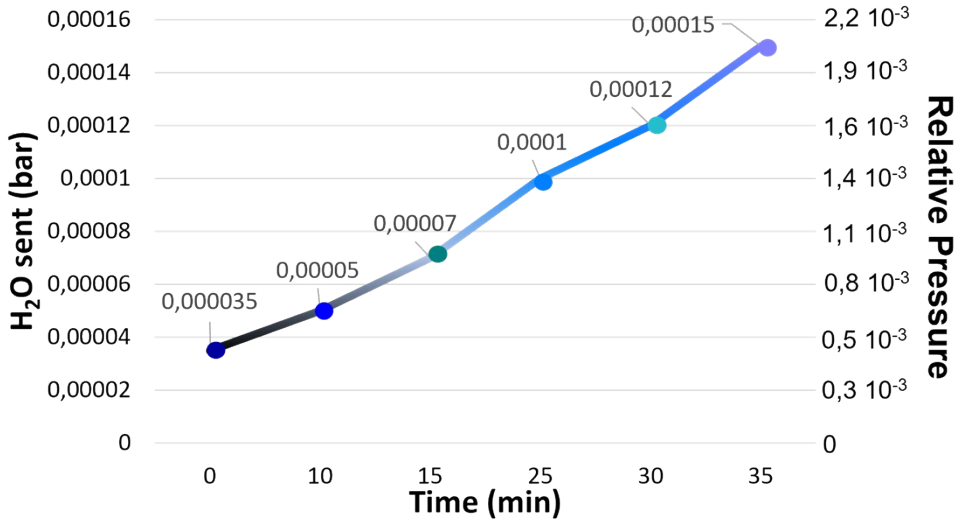

Figure S41. Schematic representation of the incremental pressures of H_2O dosed in time during the IR experiment (See Figure 6 in the main text) reported in bar and in relative pressure, assuming a local temperature of around 313 K under the IR beam (vapour pressure of H_2O at 313 K is 0.074 bar).

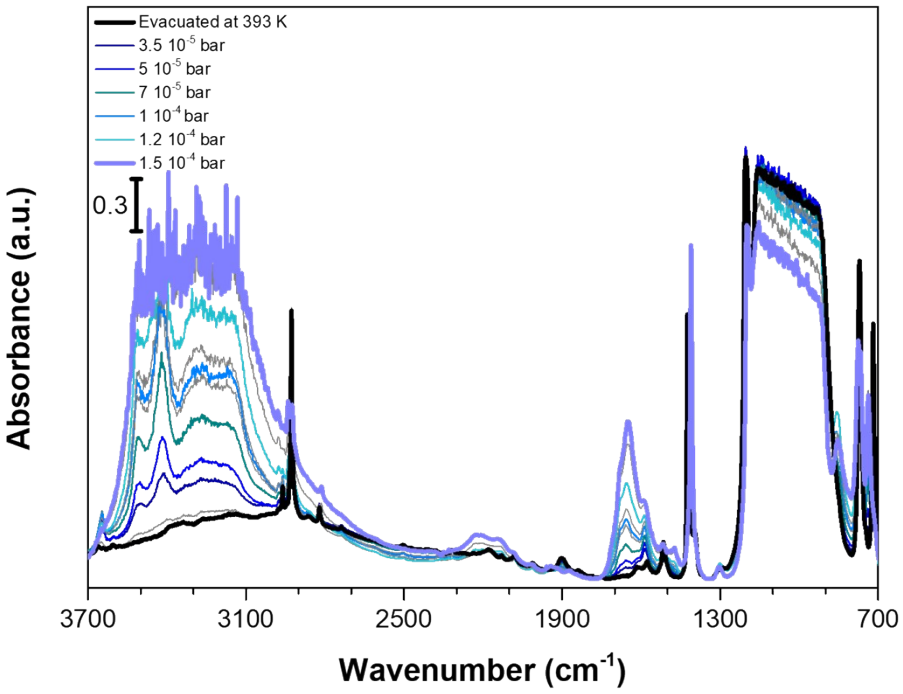

Figure S42. IR spectra of Cu-EtP collected dosing 0.35-1.5 10^{-4} bar of H_2O on the sample evacuated at 393 K, reported in the full spectral range after a baseline correction.

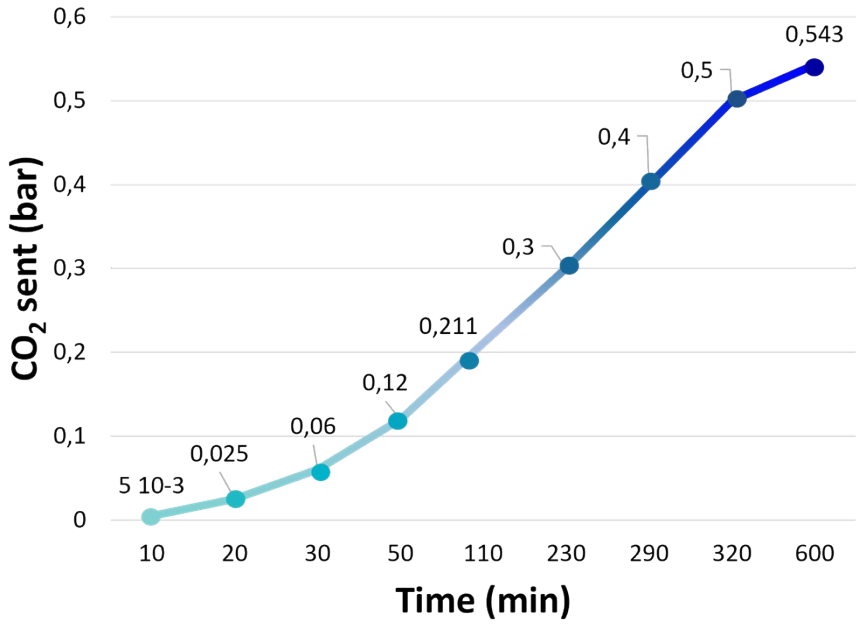

Figure S43. Schematic representation of the incremental pressures of CO_2 dosed in time during the IR experiment (See Figure 7 in the main text)

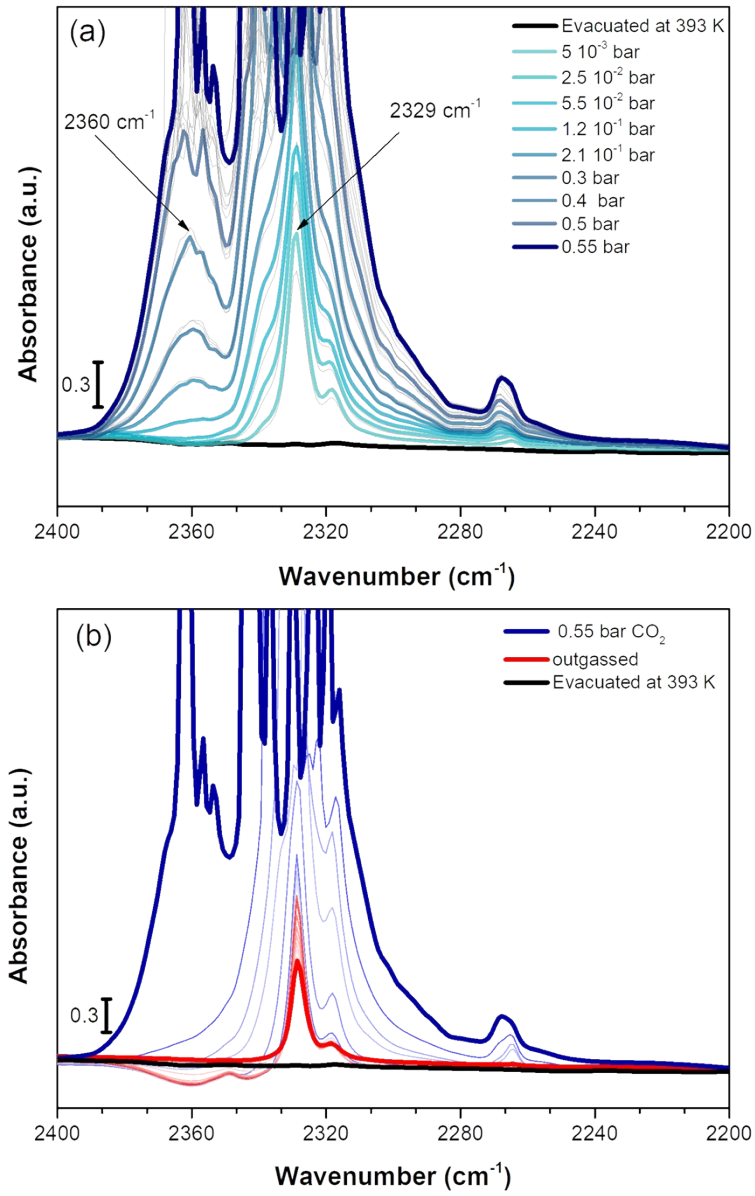

Figure S44. IR spectra in the 2400-2200 cm^{-1} spectral ranges of: CO_2 adsorption on Cu-EtP evacuated at 393 K (a) and of CO_2 desorption on Cu-EtP (b), both reported without any spectral manipulation. Blue curve represents 0.55 bar of CO_2 dosed on Cu-EtP, black curve represents Cu-EtP sample evacuated at 273 K, red curve represents the sample after a prolonged evacuation (overnight) and thinner coloured curves the intermediate pressure stages.

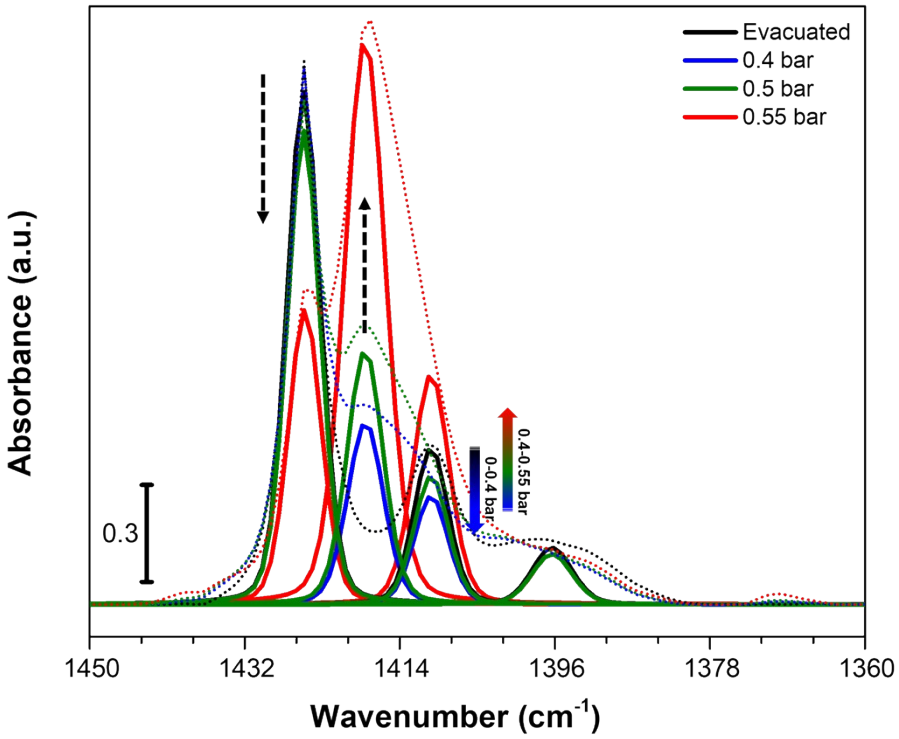

Figure S45. IR spectral deconvolution of the main bands present in the 1450-1360 cm^{-1} spectral ranges after CO_2 adsorption on Cu-EtP previously evacuated at 393 K. The evacuated sample, the 0.4, 0.5 and 0.55 bar of CO_2 coverage were chosen for the spectral deconvolution. Dotted curves represent the IR spectra of the sample at the different coverages, continuous coloured lines represent the deconvoluted spectral bands. The arrows represent the main variations observed in the spectra.

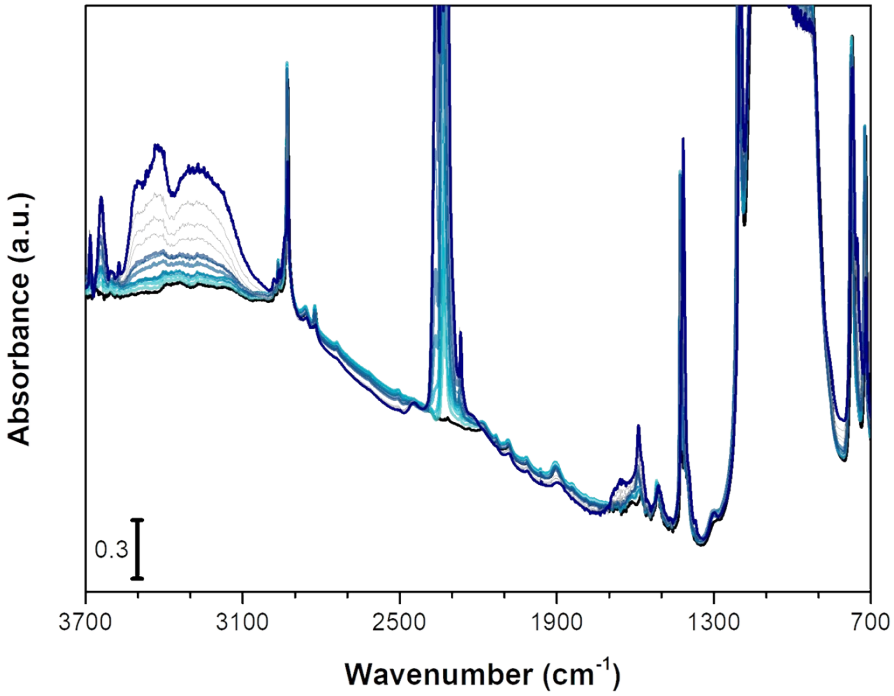

Figure S46. IR spectra of CO_2 adsorption on Cu-EtP evacuated at 393 K reported in the 3700-700 cm^{-1} spectral range reported without any spectral manipulation. The incremental pressure doses of CO_2 employed during the IR experiment are reported with thicker coloured curves.

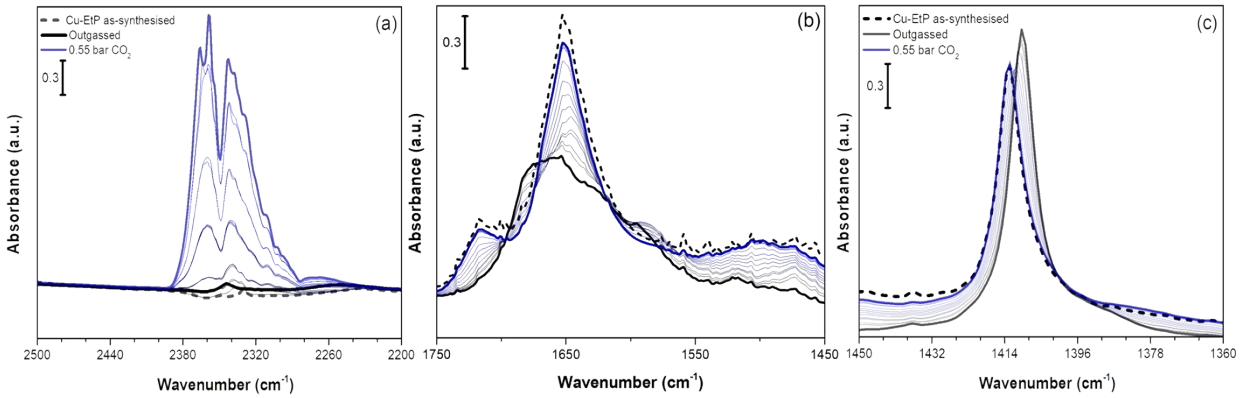

Figure S47. IR spectra of CO_2 adsorption on Cu-EtP outgassed at RT reported in the 2500-2200 cm^{-1}(a) 1750-1450 cm^{-1} (b) and 1450-1360 cm^{-1} (c) spectral ranges. Dashed black curve represents the as synthesised Cu-EtP, black curve represents the ougassed sample, blue curve represents 0.55 bar of CO_2 dosed on Cu-EtP and thinner coloured curves the intermediate pressures.

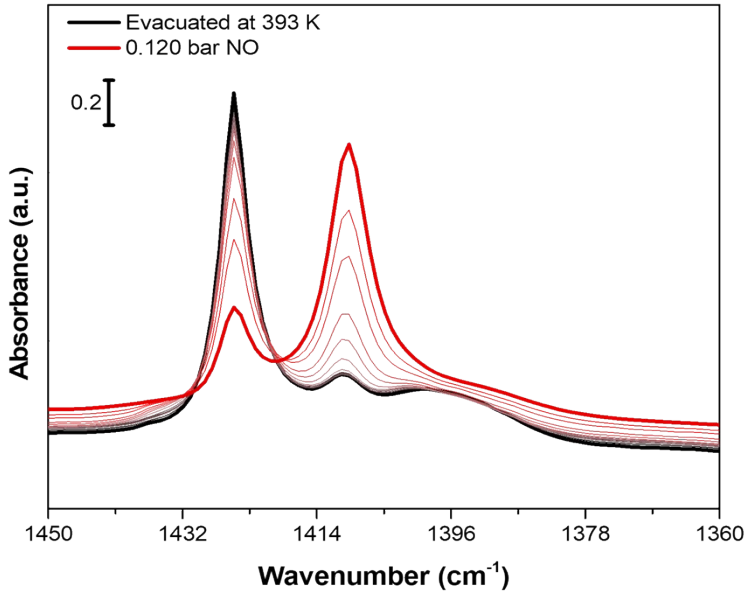

Figure S48. IR spectra of Cu-EtP after adsorption of 0.122 bar of NO in the 1450-1360 cm^{-1} spectral region on the fully activated sample (i.e. evacuated at 393 K). Black curve represents the evacuated sample, red curve represents 0.120 bar of NO dosed on Cu-EtP measured after 12 h and thinner coloured curves the intermediate pressures reached during outgassing.

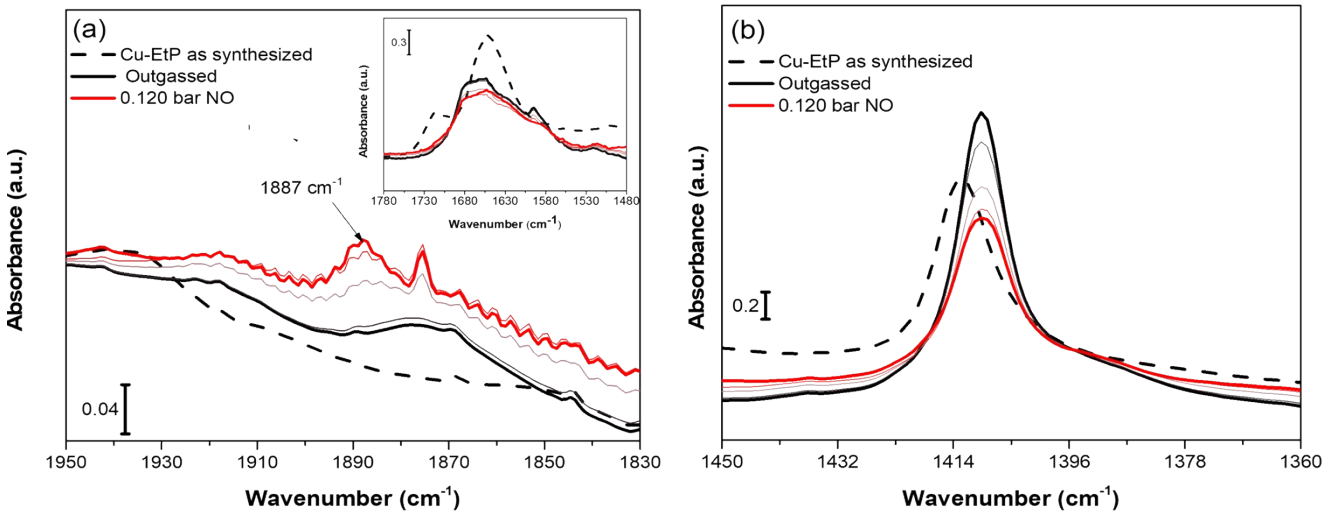

Figure S49. IR spectra of outgassed Cu-EtP after adsorption of 0.122 bar of NO at beam temperature and following outgassing in the: 1950-1830 cm-1 spectral region (a) and in the 1450-1360 cm^{-1} one (b). Dashed black curve represents the as synthesised Cu-EtP, black curve represents the outgassed sample, red curve represents 0.120 bar of NO dosed on Cu-EtP and measured after 2 h and thinner coloured curves the intermediate pressures reached during outgassing.

5. Optical spectroscopy

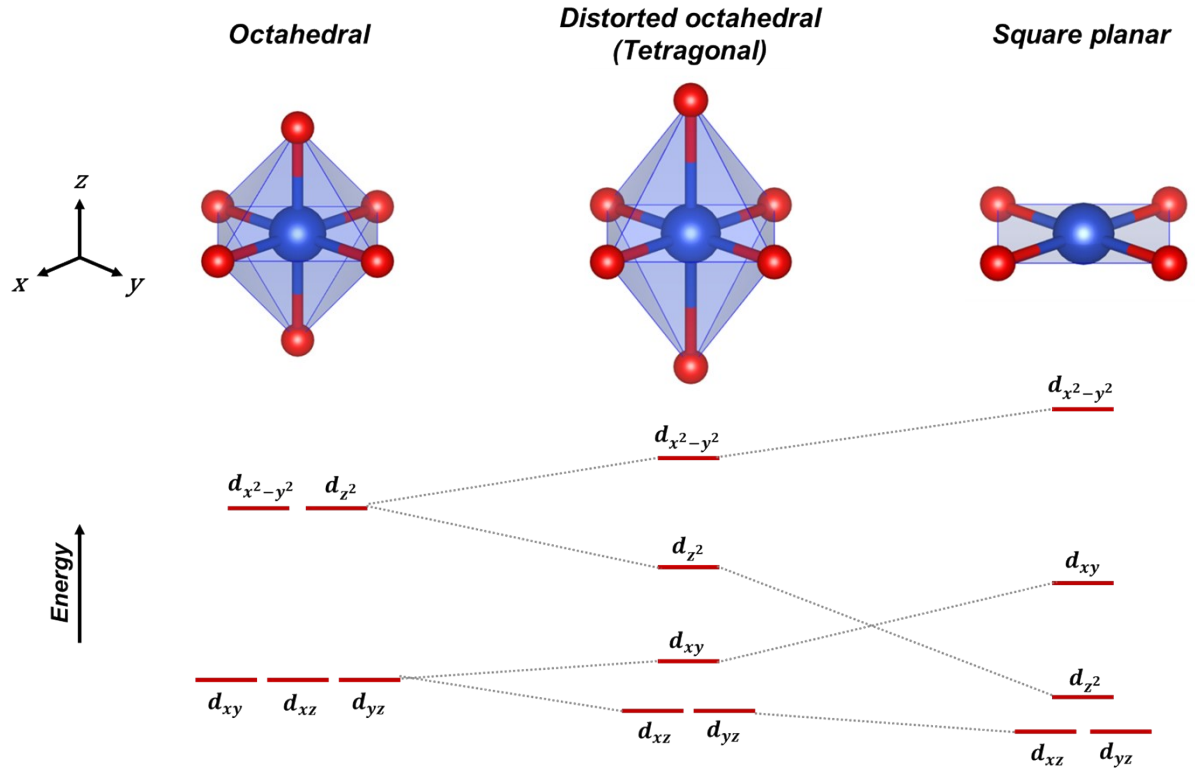

Figure S50. Splitting of *d* orbitals in octahedral, distorted octahedral (*i.e.,* tetragonal) and square planar geometry, as predicted by crystal field theory.[1] The change of coordination geometry causes clear changes in the energies of *d* orbitals. In a perfect octahedral ligand field, the *d* orbitals split in two groups, having those with t_{2g} symmetry (d_{xy}, d_{xz}, d_{yz}) lower energy compared those with e_g one ($d_{x^2-y^2}$, d_{z^2}), In Cu^{II}, having d^9 electron configuration, a single *d*-*d* transition $t_{2g} \rightarrow e_g$ would be expected for this coordination geometry. By increasing the distance of the apical ligands from the metal centre, while equatorial ones remain equivalent, the degeneracy of *d* states is partly resolved as expected by Jahn-Teller effect. In this distorted octahedral (*i.e.,* tetragonal) coordination geometry, states are more influenced by the interaction with ligands along the *z*-axis (d_{xz}, d_{yz}, d_{z^2}) are stabilised, whereas *d* orbitals laying on the *xy* plane (d_{xy}, $d_{x^2-y^2}$) get destabilised. The obtained splitting makes possible three distinct *d*-*d* transitions, whose absorption energies follow the $d_{z^2} \rightarrow d_{x^2-y^2} < d_{xy} \rightarrow d_{x^2-y^2} < d_{xz}/d_{yz} \rightarrow d_{x^2-y^2}$ trend. The elimination of the apical ligands from the coordination sphere of the metal cation (leading to a square planar coordination geometry) leads to the further stabilisation of the d_{z^2} orbital, whereas the $d_{x^2-y^2}$ and d_{xy} orbitals are destabilized by a similar extent. Finally, the energy of the d_{xz} and d_{yz} orbitals remain closely unvaried. In terms of associated electronic transitions, the $d_{xz}/d_{yz} \rightarrow d_{x^2-y^2}$ keeps approximately the same absorption energy as in the distorted octahedral geometry, whereas in the $d_{xy} \rightarrow d_{x^2-y^2}$ and $d_{z^2} \rightarrow d_{x^2-y^2}$ ones this is expected to increase,[1] so that the absorption energy trend becomes $d_{xy} \rightarrow d_{x^2-y^2} < d_{z^2} \rightarrow d_{x^2-y^2} < d_{xz}/d_{yz} \rightarrow d_{x^2-y^2}$.

6. Periodic density functional theory (DFT) simulations

Table S8. Crystallographic parameters for the DFT simulated as synthesised, evacuated and CO_2 loaded Cu-EtP.

	As synthesised	Evacuated	CO_2 loaded
***a* (Å)**	8.228	8.166	8.045
***b* (Å)**	8.313	8.167	8.383
***c* (Å)**	4.289	4.067	4.327
***α* (°)**	94.303	96.052	93.697
***β* (°)**	93.826	96.062	94.552
***γ* (°)**	45.826	49.916	50.297
Volume (Å^3)	209.78	206.15	223.78

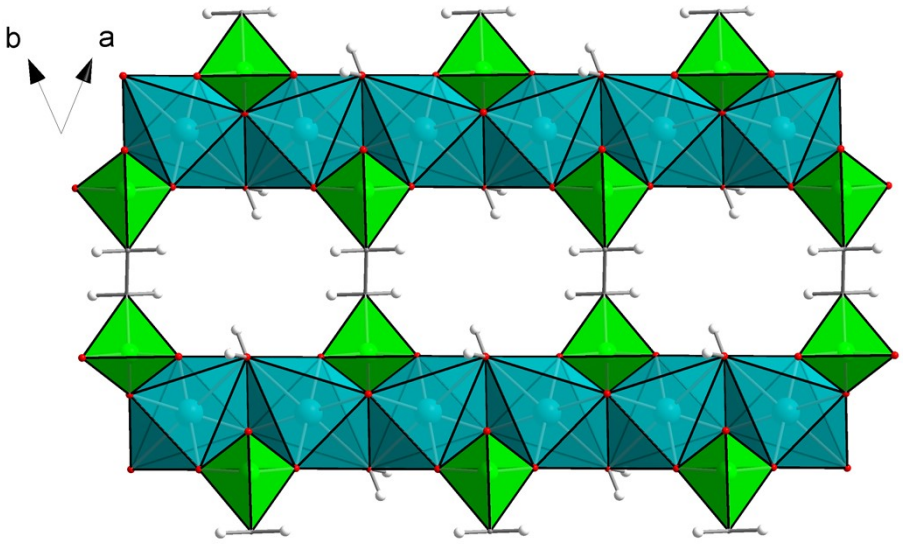

Figure S51. Polyhedral representation of the DFT optimised crystal structure of as synthesised Cu-EtP, viewed along the *c* axis. Colour code: Cu, cyan; P, green; C, grey; O, red; H, white

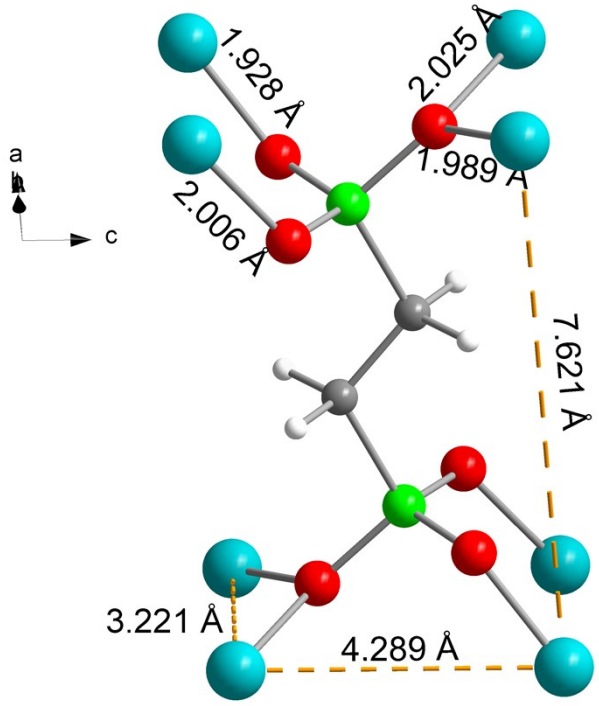

Figure S52. Local connectivity around the organic linker in the DFT optimised crystal structure of as synthesised Cu-EtP, displaying the PO-Cu distances and the Cu-Cu distances (represented as dashed orange lines) along the [110] direction (7.621 Å), the [-110] direction (3.221 Å) and the [001] direction (4.289 Å). Colour code: Cu, cyan; P, green; C, grey; O, red; H, white

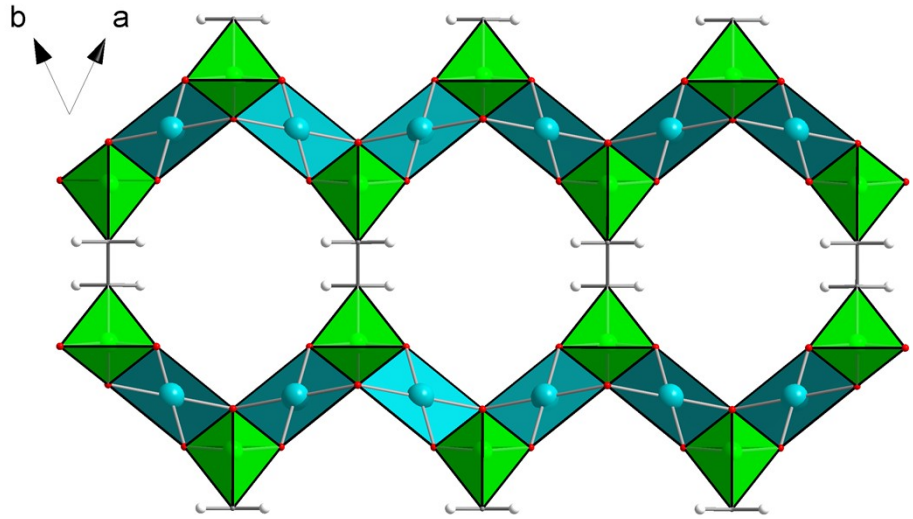

Figure S53. Polyhedral representation of the DFT optimised crystal structure of evacuated Cu-EtP, viewed along the *c* axis. Colour code: Cu, cyan; P, green; C, grey; O, red; H, white

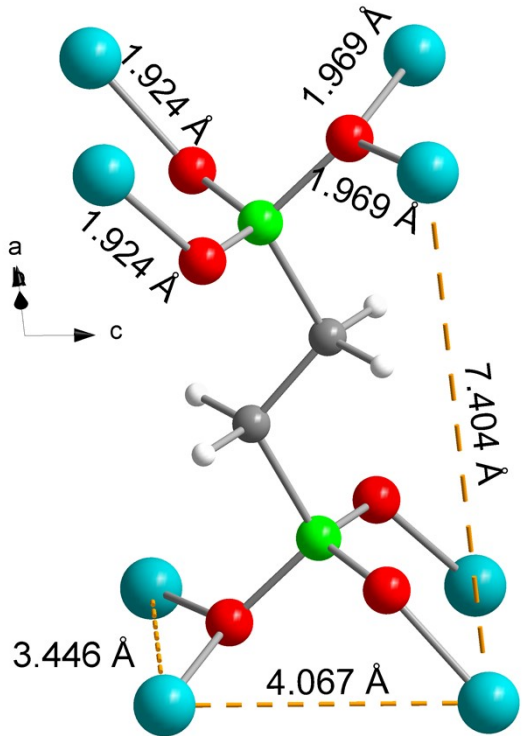

Figure S54. Local connectivity around the organic linker in the DFT optimised crystal structure of evacuated Cu-EtP, displaying the PO-Cu distances and the Cu-Cu distances (represented as dashed orange lines) along the [110] direction (7.404 Å), the [-110] direction (3.446 Å) and the [001] direction (4.067 Å). Colour code: Cu, cyan; P, green; C, grey; O, red; H, white

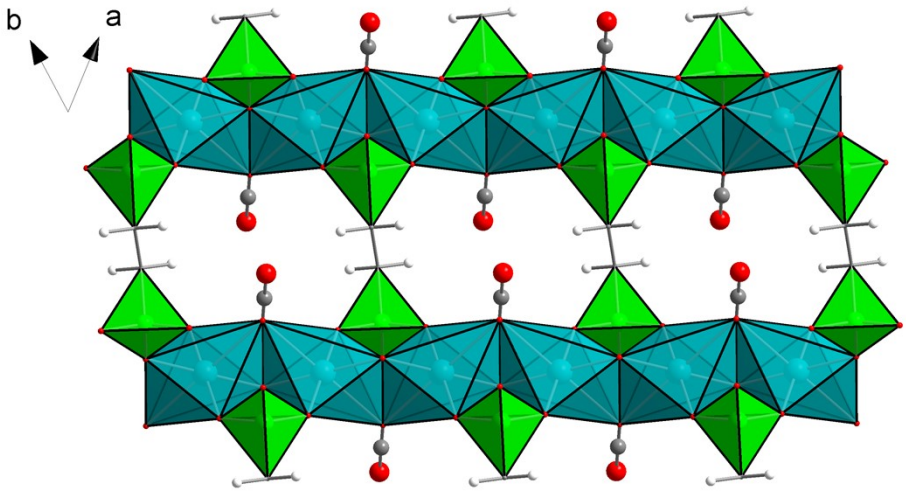

Figure S55. Polyhedral representation of the DFT optimised crystal structure of CO_2 loaded Cu-EtP, viewed along the *c* axis. Colour code: Cu, cyan; P, green; C, grey; O, red; H, white

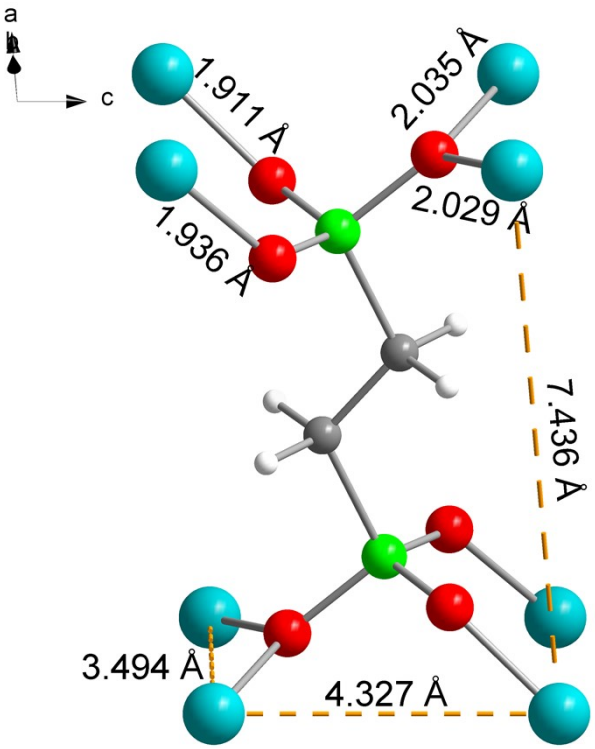

Figure S56. Local connectivity around the organic linker in the DFT optimised crystal structure of CO_2 loaded Cu-EtP, displaying the PO-Cu distances and the Cu-Cu distances (represented as dashed orange lines) along the [110] direction (7.436 Å), the [-110] direction (3.494 Å) and the [001] direction (4.327 Å). Colour code: Cu, cyan; P, green; C, grey; O, red; H, white

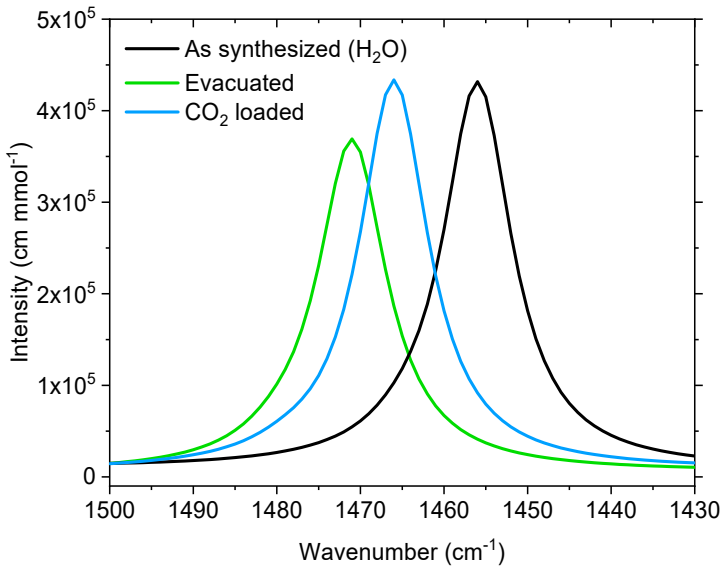

Figure S57. Simulated IR spectra of Cu-EtP for the as synthesised, evacuated and CO_2 loaded models in the $\delta(CH_2)$ region.

Table S9. Surface area for the ss synthesised and evacuated models simulated with the Zeo++ software, by considering different probe diameters.

	ASA (m^2g^{-1})[a]		NASA (m^2g^{-1})[b]	
Probe diameter (Å)	**As synthesised**	**Evacuated**	**As synthesised**	**Evacuated**
2.0	0	612	5	0
2.4	0	426	0	0
2.8	0	262	0	0
3.2	0	0	0	35
3.6	0	0	0	0

[a] Accessible Surface Area
[b] Not Accessible Surface Area

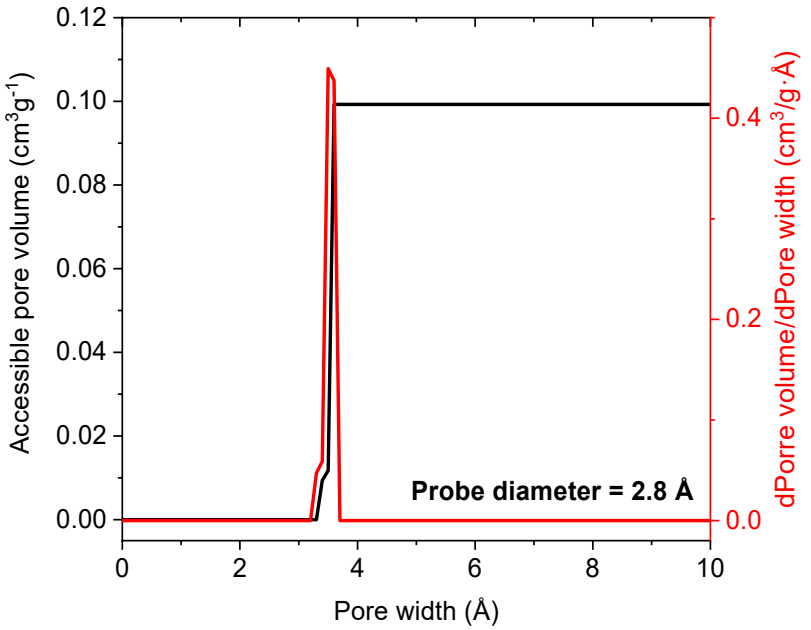

Figure S58. Pore size distribution, simulated with Zeo++ for the Evacuated model, assuming a probe diameter of 2.8 Å.

7. Supplemental references

1 W. Manch and W. C. Fernelius, *J. Chem. Educ.*, 1961, **38**, 192.